· U C ·

Faculdade de Farmácia

Universidade de Coimbra

A Novel *MYO7A* Compound Heterozygous Mutation in an USH1 Portuguese Patient: a Translational Multidisciplinary Study.

Dissertação apresentada à Faculdade de Farmácia da Universidade de Coimbra, para cumprimento dos requisitos necessários à obtenção do grau de Mestre em Biotecnologia Farmacêutica, realizada sob a orientação científica do Doutor Filipe Silva (Faculdade de Medicina, Universidade de Coimbra) e do Professor Doutor João Nuno Moreira (Faculdade de Farmácia, Universidade de Coimbra)

Nelson Monteiro, 2015

On front page:

Molecular mechanisms of Usher Syndrome. Top- Molecular biology central dogma (adapted from http://i.ytimg.com/vi/lSqUDu4zb5k/maxresdefault.jpg). **Bottom left-** the hearing (from http://laysom.com.br/wp-content/uploads/2014/08/perda-auditiva-neurossensorial.jpg). **Bottom right-** The vision (Adapted from http://www.wipak.com/company/mission/en_GB/index/_files/8124500292917l997/default/6_Mission_vision.jpg).

Agradecimentos

A realização deste trabalho não seria possível sem todo o apoio, paciência, incentivo e colaboração de um grupo de pessoas pelo qual tenho um apreço inestimável. A todas elas um muito obrigado por terem colaborado e tornado possível a conclusão de mais uma etapa da minha vida.

Em primeiro lugar quero agradecer ao Doutor Filipe Silva por ter feito com que o meu interesse pela ciência crescesse cada vez mais a cada dia. A forma como me ensinou, incentivou a pesquisar, o rigor exigido e as longas discussões quase filosóficas contribuíram sem dúvida para este crescimento. Por tudo isto, mas também pela atenção, paciência e preocupação não tenho palavras para demonstrar a minha gratidão e apreço.

Agradeço também ao Professor João Nuno Moreira, também orientador desta tese, pelo apoio e disponibilidade ao longo deste ano.

Ao Professor Henrique Girão agradeço imenso toda a ajuda, disponibilidade, interesse, sentido crítico e por me incluir na sua equipa, um enorme obrigado.

À Professora Manuela Grazina pela simpatia sempre demonstrada e por ter disponibilizado muitos meios do seu laboratório sem os quais este trabalho não seria possível.

Ao Doutor Steve Catarino e à Mestre Maria João Santos a quem agradeço tudo o que me ensinaram, toda a paciência e acima de tudo a disponibilidade e interesse demonstrado para com o meu trabalho, sem dúvida que a sua ajuda trouxe a este trabalho um grande valor.

Ao Doutor João Carlos, obrigado pela possibilidade que me deu de conhecer melhor estes doentes, sem dúvida que faz toda a diferença conhecer a verdadeira realidade de quem vive com esta doença e do seu dia-a-dia e saber que o nosso poderá um dia mudar o seu mundo para melhor é uma motivação extra para continuar sempre a dar o melhor de nós.

À Filipa Ferreira, a melhor companheira de trabalho que poderia ter tido e que mesmo longe esteve presente. Obrigado pela paciência, disponibilidade, mas acima de tudo pelas gargalhadas que tornavam mais alegres os nossos dias de trabalho.

A todos os G(u)IC pelo companheirismo no laboratório, em especial à Carla Marques, à Mónica, à Maria João e à Teresa pelas conversas, conselhos, ensinamentos e disponibilidade.

À equipa e colaboradores do laboratório de Bioquímica Genética, principalmente à Carolina Ribeiro, ao João Pratas, à Carla e ao José Albuquerque por todo o apoio.

Aos doentes e familiares agradeço a contribuição e disponibilidade que tiveram para participar neste estudo, bem como à Dra Isabel Marques do Serviço de Hematologia do CHUC pelas fornecimento das amostras controlo.

Ao IPST e ao serviço de anatomia patológica dos CHUC.E.P.E. pela disponibilidade que apresentaram em me permitir usar as suas instalações e equipamentos.

Aos meus amigos de longa data João, Mário, Francisco, Nobre, Mariana, Adriana, Raquel, Joana e Tânia um grande obrigado pela amizade sincera que Coimbra veio reforçar.

Aos amigos que Coimbra me deu, em especial aos BB's aos quais tenho imenso a agradecer. Entre eles há alguns que não posso deixar de destacar. O Rui Gomes, amigo incondicional, sempre ao meu lado até ao fim, obrigado por me ter aturado e por todo o apoio. O Bruno Marques, um verdadeiro companheiro para todos os momentos quer de trabalho quer de diversão, obrigado pela sincera e verdadeira amizade em todos os momentos. À Rute, pela genuinidade, pelos longos telefonemas e pelo apoio incondicional. À Rita Sá Ferreira, que mais que uma colega de trabalho, uma grande amiga que foi sem dúvida um pilar neste percurso, obrigado por todo o companheirismo amizade e paciência. Ao Rui Simões, à Marta, à Sofia, à Inês, à Natal e à Rovia pela amizade e por me permitirem abstrair do trabalho quando foi preciso. À Rita Moreira, à Maria João, ao Fernando e ao Manolo que mesmo longe mostraram que a amizade não se mede pela distância.

Obrigado à Catarina, à Joana, ao João, à Helena e à Vânia pela amizade e companheirismo.

À Inês Tavares e ao Bernardo tenho que agradecer por tornar o meu dia mais agradável ao chegar a casa, obrigado por todas as gargalhadas.

Por último, mas de todo não menos importante, à minha Família. Ao meu cunhado, tios e primos, obrigado por todo apoio que me deram ao longo deste percurso, sem vocês seria muito mais difícil. Aos meus sobrinhos, que embora não tenham noção, foram um grande suporte neste trabalho, porque com eles nada mais parece existir.

À minha irmã, um grande pilar em toda a minha existência, tenho que lhe agradecer muito daquilo que sou, obrigado por todas as picardias, gargalhadas e teimosias. Obrigado por cuidares de mim, por me apoiares incondicionalmente e por não me deixares desistir. Desculpa as minhas ausências mas nem sempre foi fácil.

Aos meus pais, aos quais quase me faltam as palavras para descrever o quão agradecido estou. Obrigado pelo apoio incondicional, por tudo o que me ensinaram, por me fazerem manter os meus princípios e por fazerem com que os tenha. Obrigado por serem o meu porto de abrigo, tudo o que sou hoje a vocês devo e se muitas vezes marquei pela

ausência quero me desculpar, mas estava a lutar pelos meus objectivos de entre os quais está deixar-vos orgulhosos. Nunca esquecerei o vosso esforço para que este momento se tornasse real.

A todos um sincero obrigado!

Aos meus pais.

Index

Tables index

Figures Index

Abbreviations

A	Adenine
bp	Base pair
C	Cytosine
cDNA	Complementary Deoxyribonucleic acid
CEU	Utah residents with Northern and Western European ancestry
del	Deletion
DMEM	Dulbecco's Modified Eagle Medium
DNA	Deoxyribonucleic acid
DNAse	Desoxirribonuclease
dup	Duplication
ECL	Enhanced chemiluminescence
EDTA	Ethylenediamine tetraacetic acid
ERG	Electroretinogram
FBS	Fetal bovine serum
FERM	Four-point-one, ezrin, radixin, moesin domain
Fw	Forward
Fig.	Figure
G	Guanine
GCL	Ganglion cell layer
GFP	Green fluorescent protein
GFP-myo7a(F3)wt	C-terminus MyTH4-FERM wt domains tagged with Green fluorescent protein (GFP)
GFP-myo7a(F3)mut	C-terminus MyTH4-FERM with c.5561dupT domains tagged Green fluorescent protein (GFP)
h	Hour
HEK-293	Human Embryonic Kidney 293 cell line,
Het	Heterozygous
HRP	Horseradish peroxidase
INL	Inner nuclear layer
IPL	Inner plexiform layer
kDa	kiloDalton
LB	Luria-Bertani

min	Minute(s)
MyTH4	Myosin Tail Homology 4 domain
n	Number of subjects
NCBI	National Center for Biotechnology Information
NP-40	Nonyl phenoxypolyethoxylethanol
ONL	Outer nuclear layer
OPL	Outer plexiform layer (OPL)
PCR	Polymerase Chain Reaction
PMSF	Phenylmethanesulfonyl fluoride
RCF	Relative centrifugal force and is expressed in units of gravity
Rev	Reverse
RFLP	Restriction fragment length polymorphism
RGCs	Retinal ganglion cells
RIN	RNA integrity number
RIPA	Radioimmunoprecipitation assay
RNA	Ribonucleic acid
RNAse	Ribonuclease
RP	Retinitis pigmentosa
RPE	Retinal pigment epithelium.
RT-PCR	Reverse transcriptase-polimerase chain reaction
SDS	Sodium dodecyl sulfate
SDS-PAGE	Polyacrylamide gel containing sodium dodecyl sulfate
sec	Second(s)
SH3	SRC Homology 3 Domain
SNHL	Sensorineural hearing loss
T	Timine
TBE	Tris Borate EDTA
TBS	Tris-buffered saline
TBS-T	Tris-Buffered Saline and Tween 20
USH	Usher syndrome
USH1	Usher syndrome type one
USH2	Usher syndrome type two
USH3	Usher syndrome type three
UV	Ultraviolet

Wt	Wild-type
WHO	World Health Organization

Abstract

Usher syndrome is an autosomal recessive disease characterized by the association of retinitis pigmentosa and sensorineural hearing loss with or without vestibular dysfunction. Prevalence for this disease was estimated to be 3-4 per 100,000 individuals.

Distinguished by clinical features, Usher syndrome can be divided in three types, where Usher syndrome type 1 is the most severe form. Causing disease mutations were reported in 10 genes, 6 of them associated to Usher syndrome type I. *MYO7A* gene is the most commonly mutated gene for this type, representing approximately 50% of the cases. *MYO7A gene* codes for myosin VIIa protein, previously described as a motor transport protein and participating in the establishment of cell-cell adhesions.

This work aimed to evaluate the possibility of two novel *MYO7A* variants, identified in compound heterozygosity in a Usher syndrome type 1 Portuguese patient using a Targeted resequencing approach to 9 of the Usher syndrome associated genes, be responsible for the phenotype.

Accordingly, the segregation analysis of these variants (c.3503+1delG and c.5561dupT) in the available patient relatives was performed, as well as the analysis of other five variants located between the two variant *loci*. Furthermore, 250 samples from normal individuals were analysed for the two novel variants and all of them presented the normal genotypes.

Additionally, an *in silico* study was performed aiming to evaluate the evolutionary conservation of the two variant *loci*, revealing that the first is highly conserved among the mammalian analysed species while the second is highly conserved among the vertebrate analysed species. Since *MYO7A* c.3503+1delG variant is located at the donor splice site of *MYO7A* exon 27, alteration of splice site analysis was performed with *in silico* Splice site prediction and the complete absence of the normal donor splice site at *MYO7A* exon 27 was observed. Altogether, these results support the hypothesis that the two variants (c.3503+1delG and c.5561dupT) can be a compound heterozygous mutation responsible for Usher syndrome type I phenotype in the studied patient.

In order to confirm the presence of the two variants in the *MYO7A* transcript nucleotide sequences, nasal epithelium samples from the patient and two normal individuals were studied and both wt and c.5561dupT alleles were expressed, while c.3503+1delG was only identified as the wt allele. However, it is predictable that a complex phenomenon be occurring at this splice site due to c.3503+1delG mutation. Finally, considering that it is

predictable that c.5561dupT mutation causes a *MYO7A* frameshift leading to a truncated myosin VIIa protein with a partially abnormal second MyTH4 domain and completely without the second FERM domain and the protein C-terminus, it seemed relevant to understand the effect of such mutation at the cellular and molecular level. Therefore, protein-protein interaction studies were performed with two constructions of C-terminal MyTH4-FERM (wt and mut), tagged with GFP. These studies suggested that the previously reported interaction of myosin VIIa with myrip was preserved in the presence of the MyTH4-FERM mut, and a gain of myosin VIIa function was achieved with the MyTH4-FERM mut, which seems to interact with munc13-4 protein, an interaction that was not seen with the MyTH4-FERM wt. Co-localization of both myosin VIIa with MyTH4-FERM mut and munc13-4 proteins was observed near vesicles structures when both were simultaneously expressed in HEK293a cells.

This study reveals that *MYO7A* c.3503+1delG and c.5561dupT mutations are a compound heterozygous mutation causing USH1 in a Portuguese patient, and elucidate some functional myo7a protein alterations that may be important to understand the molecular mechanisms of this disease. However, further studies are required to clarify these implications at the cellular level.

Resumo

O Síndrome de Usher é uma doença autossómica recessiva caracterizada pela associação de duas patologias, retinite pigmentosa e da perda auditiva sensoneural, às quais poderá estar também associada uma disfunção vestibular. Estima-se que esta doença afecta 3 a 4 indivíduos em cada 100 000.

Distinguidos pelas características clínicas, o Síndrome de Usher pode ser dividido em três tipos, de entre os quais o Síndrome de Usher do tipo 1 é a forma mais severa. Até à data foram identificados 10 genes que possuem mutações causadoras desta doença, 6 dos quais foram associados ao Síndrome de Usher do tipo 1. O gene MYO7A é o gene onde foram encontradas mais mutações em doentes com este tipo de síndrome, representando cerca de 50% dos casos. O gene MYO7A codifica uma proteína designada de miosina VIIa, a qual já foi previamente descrita como uma proteína transportadora que também está envolvida no estabelecimento de adesões intercelulares.

Este trabalho tem por objectivo avaliar a possibilidade de duas novas variantes do gene MYO7A serem responsáveis pelo fenótipo do Síndrome de Usher do tipo 1. Estas duas novas variantes foram identificadas em heterozigotia composta num doente português com Síndrome de Usher do tipo 1, através de uma abordagem de Targeted resequecing para 9 dos genes associados ao Síndrome de Usher.

Assim sendo, foi feita a análise não só destas variantes (c.3503+1delG e c.5561dupT) mas também de outras cinco variantes localizadas entre entes loci, nos familiares em que foi possível. Além disso, as duas novas variantes foram analisadas em 250 amostras provenientes de indivíduos saudáveis, sendo que não foram encontradas em nenhuma destas amostras.

Para além disso, com o objectivo de avaliar a conservação evolutiva destes loci foram realizados estudos in silico que demonstraram que ambos os loci são extremamente conservados entre as espécies de mamíferos analisadas. Uma vez que a variante c.3503+1delG do gene MYO7A está localizada no donor splice site do seu exão 27, foi feita uma previsão da alteração do local de splicing com um softweare online (splice site prediction), previsão esta que revelou uma completa destruição deste local de splicing na presença desta variante. Todos estes resultados sustentam a hipótese de que estas duas variantes (c.3503+1delG e c.5561dupT) possam constituir uma mutação heterozigótica composta responsável pelo fenótipo do Síndrome de Usher do tipo 1 no doente estudado.

Com o intuito de perceber se estas duas novas variantes estariam alteradas na sequência de nucleótidos do transcrito do gene MYO7A, foram utilizadas uma amostra do epitélio nasal do doente e duas amostras do epitélio nasal de dois indivíduos normais, tendo

sido verificada a expressão quer do alelo normal quer do alelo com a variante c.5561 na amostra do doente. No que diz respeito à variante c.3503+1delG, apenas foi possível identificar o alelo selvagem. Contudo, é espectável que na presença desta mutação possa estar a ocorrer um fenómeno complexo. Por último, considerando a probabilidade que a mutação c.5561dupT cause uma frameshift no transcrito do gene MYO7A, originando uma miosina VIIa truncada com um segundo domínio MyTH4 parcialmente anómalo que leva à destruição completa do segundo domínio FERM e do C-terminal da proteína, é relevante elucidar quais os efeitos desta mutação ao nível celular. Posto isto, foram realizados estudos de interacção proteína-proteína com duas construções dos domínios MyTH4-FERM do terminal carboxílico (selvagem e mutada) com uma tag de GFP. Estes estudos sugerem que a interacção já descrita entre a miosina VIIa e a myrip foi preservada na presença da mutação. Para além disso, foi identificado aquilo que parece ser um ganho de função por parte destes domínios do terminal carboxílico da miosina VII. Na presença da mutação, observou-se interacção com a munc13-4, o que não é detectado na presença destes domínios na sua forma selvagem. A ocorrência desta interacção e de um possível ganho de função na presença da mutação por parte da miosina VIIa é suportado pela observação da co-localização da muc13-4 e dos domínios do terminal carboxílico da miosina VIIa mutada perto de estruturas que se assemelham a vesículas, quando ambas são expressas nas células HEK293a.

Este estudo revela que as mutações c.3503+1delG e c.5561dupT do gene MYO7A constituem uma mutação heterozigótica composta que é causa do fenótipo de Síndrome de Usher do tipo 1 num doente Português. Para além disso, elucida algumas alterações da miosina VIIa que podem ser importantes para elucidar os mecanismos moleculares desta doença. Contudo, mais estudos serão necessários para clarificar estas implicações ao nível celular.

Chapter 1

Introduction

1. Introduction

1.1 Eye anatomy and photo transduction

The human eye is a highly specialized organ responsible for capture, adjust and transform light into chemical signals to be interpreted by the brain. It is strongly associated with the perception of the human surrounding world (Purves 2004).

The eyes (ocular system) together with their connecting pathways to the brain (neuronal system) form the visual system. The ocular system is responsible for the focus of the external visual image and the neuronal system for converting the visual image into electrical impulses transmitted to the brain through the optic nerve (Purves 2004; Kolb 2005).The eye is divided in three different layers: the external layer, constituted by the sclera and cornea; the intermediate layer, which can be divided in two parts: anterior constituted by iris and ciliary body and posterior constituted by choroid; and the internal layer constituted by retina, the sensory part of the eye (Kolb 2005). The sclera is the tension-bearing component of the eye which is essential for permanent stable shape (Ebneter, et al. 2015). The cornea is glass-like transparent, smoothness and avascular being responsible for the majority of the eye's focusing power and eye protection against physical insults and entrance of debris and infection (Levis et al. 2015). The iris is a coloured circular muscle which is responsible to control the size of the pupil (black-looking aperture that allows light to enter the eye) in order to select the quantity of light capitation. The ciliary body consists of a muscular component that is important for adjusting the refractive power of the lens and a vascular component (the so-called ciliary processes) that produces the fluid that fills the front of the eye, the aqueous humour (Purves 2004). Attached to the anterior portion of the ciliary body exists the called zonule fibers which are responsible for changing the shape of the lens, a process called accommodation that allows the eye to form a sharp image on the retina (Kolb 2005). The lens is a remarkable transparent tissue that is responsible for diffracting light so that it focuses precisely on the retina (Petrash 2013). The choroid is a vascular structure that supplies the outer retina with oxygen and nourishment (Nickla and Wallman 2010). In addition, the eye possesses three chambers of fluid: the anterior chamber (between cornea and iris), the posterior chamber (between iris, zonule fibers and lens), and the vitreous chamber (between the lens and the retina). The anterior and the posterior chambers are filled with a transparent gelatinous fluid (aqueous humour), whereas the vitreous chamber is filled with vitreous humour, a more viscous fluid (Kolb 2005). The anatomy of the eye is schematized in Figure 1.

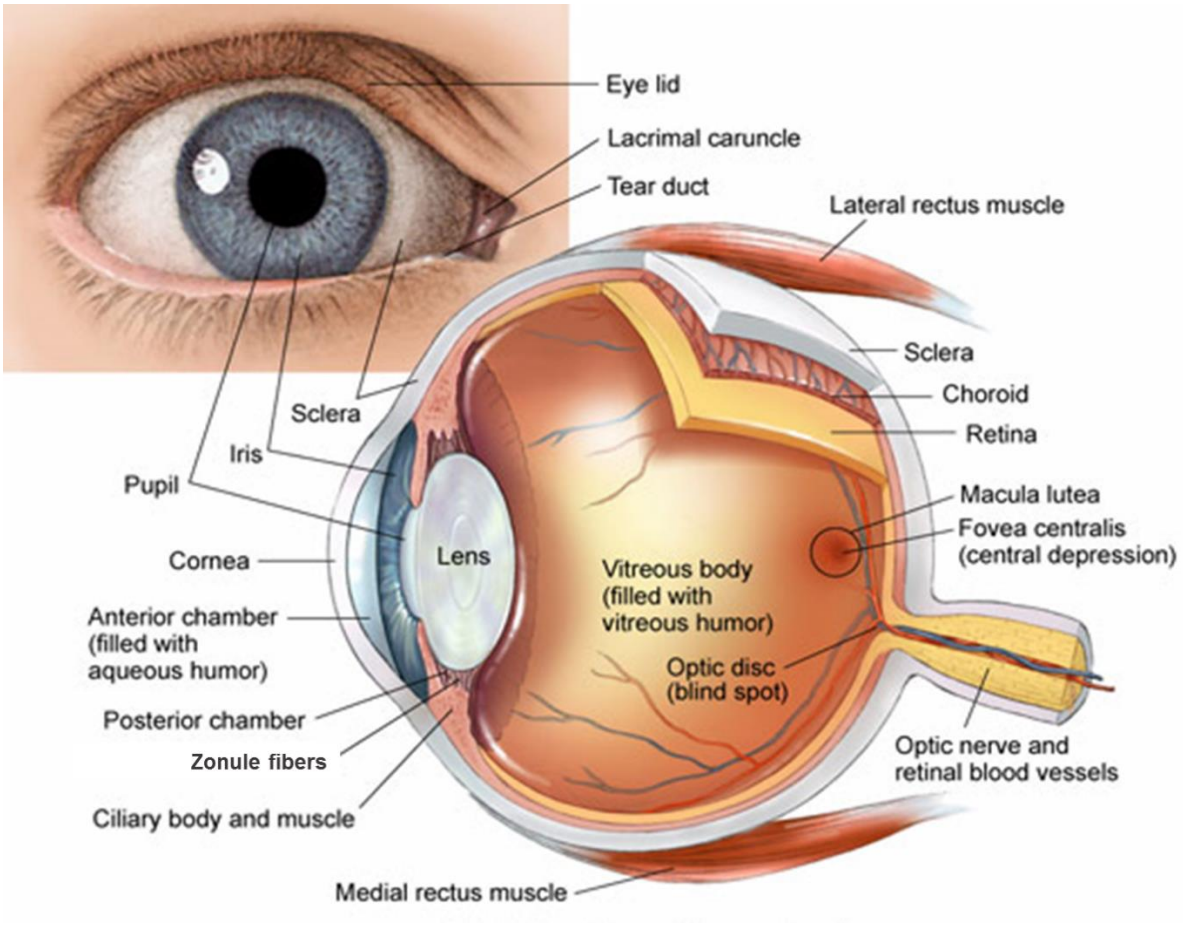

Figure 1- Anatomy of the human eye (adapted from http://www.centralfloridaretina.com/eye-anatomy/).

The retina is the neural section of the eye, located in the back of the eye, and it is the structure responsible for translate light into electric signals and enabling to see under different conditions like dark/sunlight, enabling to discriminate colours and provide a high degree of visual precision (Erskine and Herrera 2014). In the retina there are five types of neurons: photoreceptors (rods and cones), horizontal cells, bipolar cells, amacrine cells and ganglion cells (RGCs). These five types of neurons are organized in different layers in which three of them are layers of neural cell bodies and two of them are matching with the location of processes and synaptic contacts. The three layers of neuronal cell bodies are the outer nuclear layer (ONL), which comprises the photoreceptors cell bodies, the inner nuclear layer (INL), comprising the cell bodies of bipolar, horizontal and amacrine cells, and the ganglion cell layer (GCL), which comprises the cell bodies of ganglion cells and displaced amacrine cells. The other two layers are the outer plexiform layer (OPL), where the connections between photoreceptors and vertically running bipolar cells and horizontally oriented horizontal cells

occur, and the inner plexiform layer (IPL), which functions as a relay station for the vertical-information-carrying nerve cells, the bipolar cells, connect to ganglion cells (Kolb 1991; Purves 2004). The inner wall of the optic cup gives rise to the retina while the outer wall gives rise to a thin melanin-containing epithelium, the retinal pigment epithelium (RPE), which reduces backscattering of the light that enters the eye. RPE is responsible for the renewal of photoreceptors outer segment which is important to their normal function (Angeles 1967; Young and Bok 1969). A schematic representation of the retina and its structural layers and cells are shown at Figure 2A.

Photoreceptors (rods and cones) are responsible for the transduction of light energy into electrical signals. They are distinguished by the shape, the type of photo pigment they contain, distribution across the retina and pattern of synaptic connections. The rod system is specialized for sensitivity at the expense of resolution. On the other hand, the cone system has very high spatial resolution and is specialized for acuity at the expense of sensitivity. The perception of the colours is also one of the properties of the cone system. Photoreceptors are consisted of two segments: inner and outer segment (Purves 2004) (see Figure 2B). The outer segment is a modified sensory cilium which contains many tightly-packed flat membrane disks harbouring proteins involved in photo transduction. This segment undergoes active and continuous renewal with their proteins and membranes synthesized in the inner segment and transported to the outer segment by intra-flagellar transport through the connecting cilium. Adding of new disks proximally (closer to cell body) is balanced by shedding of old disks distally (more distant from cell body). Retinal pigment epithelium (RPE) cells phagocyte and digest the shed photoreceptor outer segment tips, and participate in visual pigment regeneration (Mathur and Yang 2015). Horizontal cells are the interneurons that provide the pathways for both local and long range interactions between photoreceptors (Perlman, et al. 2012). Bipolar cells are the second order neurons that constitute the vertical visual pathway. These cells receive the synaptic input from photoreceptors and transmit it to the RGCs and to the amacrine cells. Amacrine cells modulate the interactions between bipolar cells and RGCs. Human retina have about 40 different types of amacrine cells that can be distinguished by their dendritic size, stratification and neurotransmission release. The RGCs collect the visual information through their dendrites from the amacrine and the bipolar cells, and delivers it to the brain by their axons that constitute the optic nerve (Kolb 1991; Purves 2004).

In the retina, there are three types of glial cells: Müller cells, astrocytes, and microglial cells (Rosa et al. 2015). Müller cells, the principal macroglia of mammalian retina, span from the vitreal surface to sub-retinal space and cover all retinal layers. These cells, partici-

pate in several essential roles in metabolism, functions, maintenance and protection by providing trophic factors, removing metabolic wastes, controlling extracellular space volumes and, ion and water homeostasis, contributing to visual cycles, releasing neurotransmitters, regulating blood retina barrier function and modulating innate immunity (Reichenbach and Bringmann 2013). Müller glia is also a major protector to various stresses by reactive gliosis involving morphological, biochemical and physiological changes (Wang 2015). Astrocytes have homeostatic functions, including water, ions and glutamate buffering of the neurons. Additionally, play a critical role in the development of retinal vasculature and inner blood-retinal barrier maintenance (Phatnani and Maniatis 2015). Microglial cells are the resident immune cells of the central nervous system and constitute the primary response in a defence network (Lull and Block 2010). Retinal microglial cells are located near zonule fibers, GCL, as well within IPL and above INL (Bosco et al. 2011).

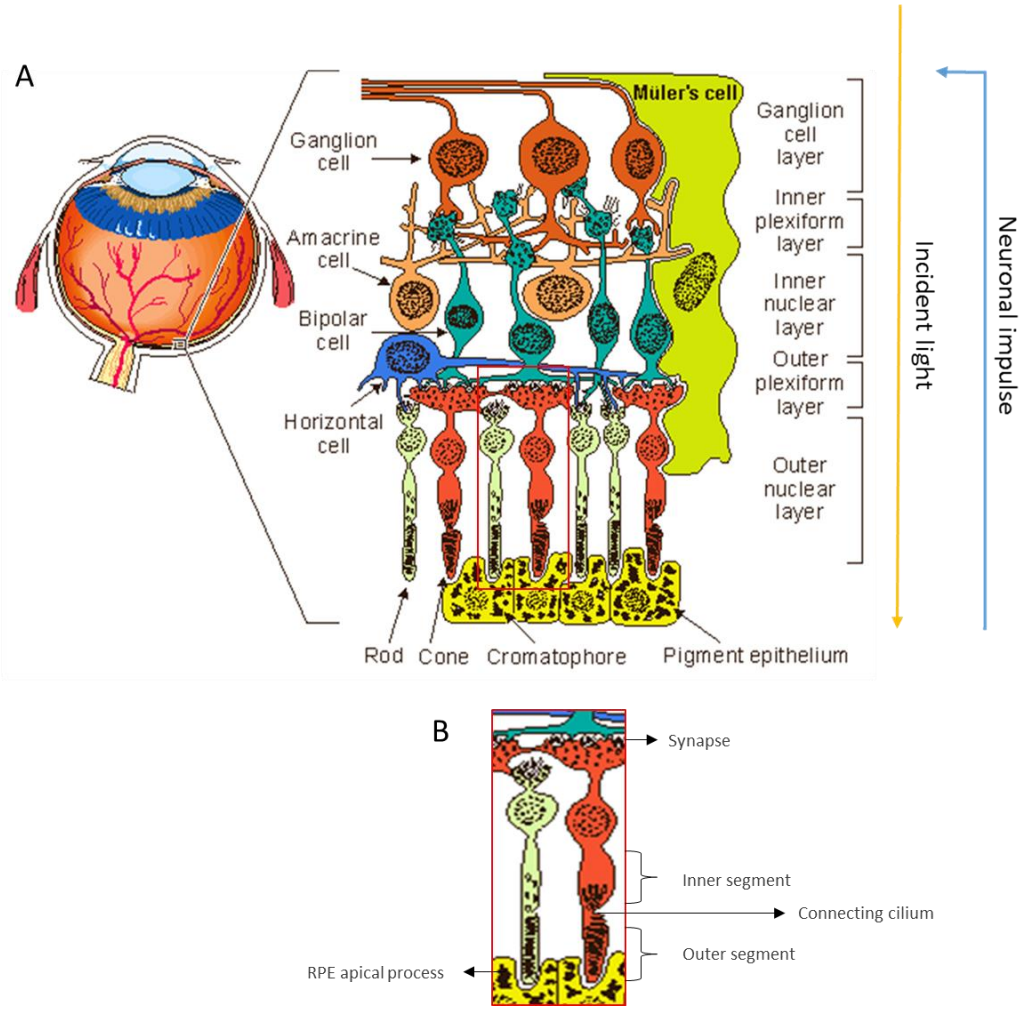

Figure 2- Retina structure. A-Structural layers and cells of the retina. In the right is represented the flow of the light course (yellow arrow) into neuronal impulse (blue arrow). **B-**Photoreceptors structure. The rod is represented in green and the cone in red (adapted from http://www.bem.fi/book/28/28.htm).

1.2 Retinitis Pigmentosa

Retinitis Pigmentosa (RP) is a major cause of visual impairment and blindness, affecting millions of people worldwide. RP refers to a group of inherited disorders clinically characterized by night blindness, often starting in puberty, followed by progressive loss of peripheral vision and subsequent loss of central vision which can culminate in complete blindness. Clinical diagnosis of RP is made if retinal examination include 'bone spicule' pigmentary deposits, retinal vessel attenuation, and characteristic changes in electroretinogram (ERG) patterns (Daiger et al. 2013).

At the cellular level, RP is characterized by a progressive dysfunction and loss of rod photoreceptors, first affecting night vision in the rod-rich mid-peripheral retina, then progressing into the cone-rich central retina, with eventual loss of cones either as a direct result of the disease process or secondary to the death of rods (Liu et al. 2015).

1.3 Ear anatomy

The ear is also involved in the perception of the human surrounding world. Hearing is essential for the development of a normal speech and surely participated in the human progress of communication.

The mammalian ear is divided in three parts: the outer, the middle and the inner ear. The outer ear is responsible for collecting sound and leading it into the ear canal to the tympanic membrane. Sound induces an oscillation in air pressure making tympanic membrane vibrate. Such vibrations are transmitted to the middle ear where three ossicles (malleus, incus and stapes), directly coupled to the oval window, also vibrate and convey the vibrations into the inner ear. The pressure of the tympanic membrane upon the oval window is not loss by signal reflection due to impedances of the compressible air in the ear canal and incompressible fluid in the inner ear (Purves 2004; LeMasurier and Gillespie 2005). The ear anatomy is schematized in Figure 3.

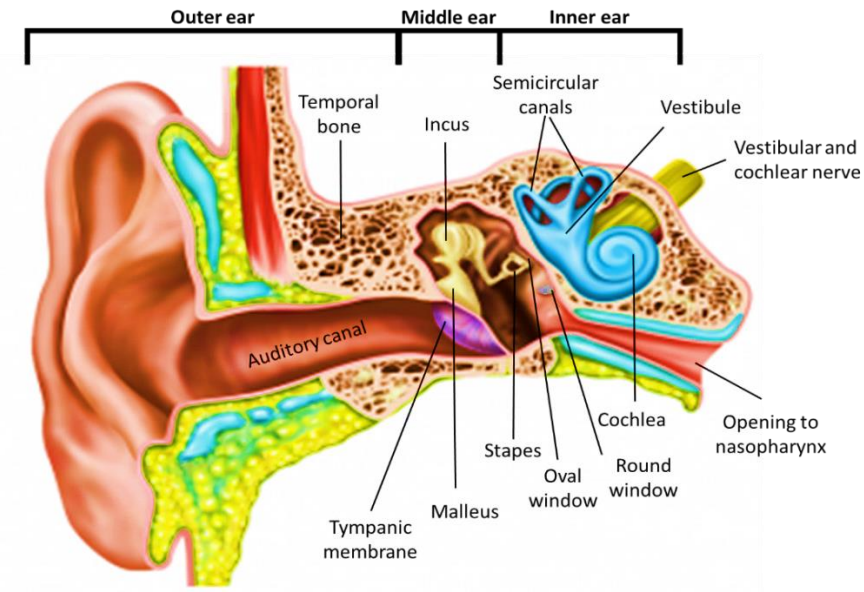

Figure 3- Ear anatomy (adapted from http://denverentblog.com/category/ears/)

The inner ear (Figure 4A) is divided in three fluid-field compartments: scala vestibuli, scala media and scala tympani. The scala vestibuli and the scala tympani bring together parts of a continuous cochlear duct with two windows opening on the middle ear, oval and round windows. The scala media is located in the centre of the cochlea separated from the scala vestibuli by Reissner's membrane and from the scala tympani by the basilar membrane (Figure 4B). The organ of Corti, which is located upon the basilar membrane, contain the sensory cells of the auditory system, the hair cells (Slepecky 1996). Hair cells are common receptors of the auditory and vestibular sensory organs and of the lateral line. In the organ of Corti, hair cells are divided in one row of inner hair cells and three rows of outer hair cells (Figure 4C) (Dallos 1992). The hair bundle, the defining feature of all hair cells, is the organelle directly responsible for mechanotransduction, in other words, responsible for the transformation of mechanical force into an electrical signal. The bundle is extremely sensitive to mechanical stimuli which are essential to convert basilar-membrane oscillations into neural impulses. Basilar-membrane oscillations cause a hair bundle deflection which initiates the mechanoelectrical transduction. This deflection induces opening of the transduction channel, a non-selective cation channel. This opening leads to hair cells depolarization, voltage-dependent Ca^{2+} channels near basolateral synapses open, the rising of Ca^{2+} levels induces the neurotransmitter release at the glutamatergic synapses and begins signal propagation to afferent neurons towards central nervous system (Purves 2004; LeMasurier and Gillespie 2005).

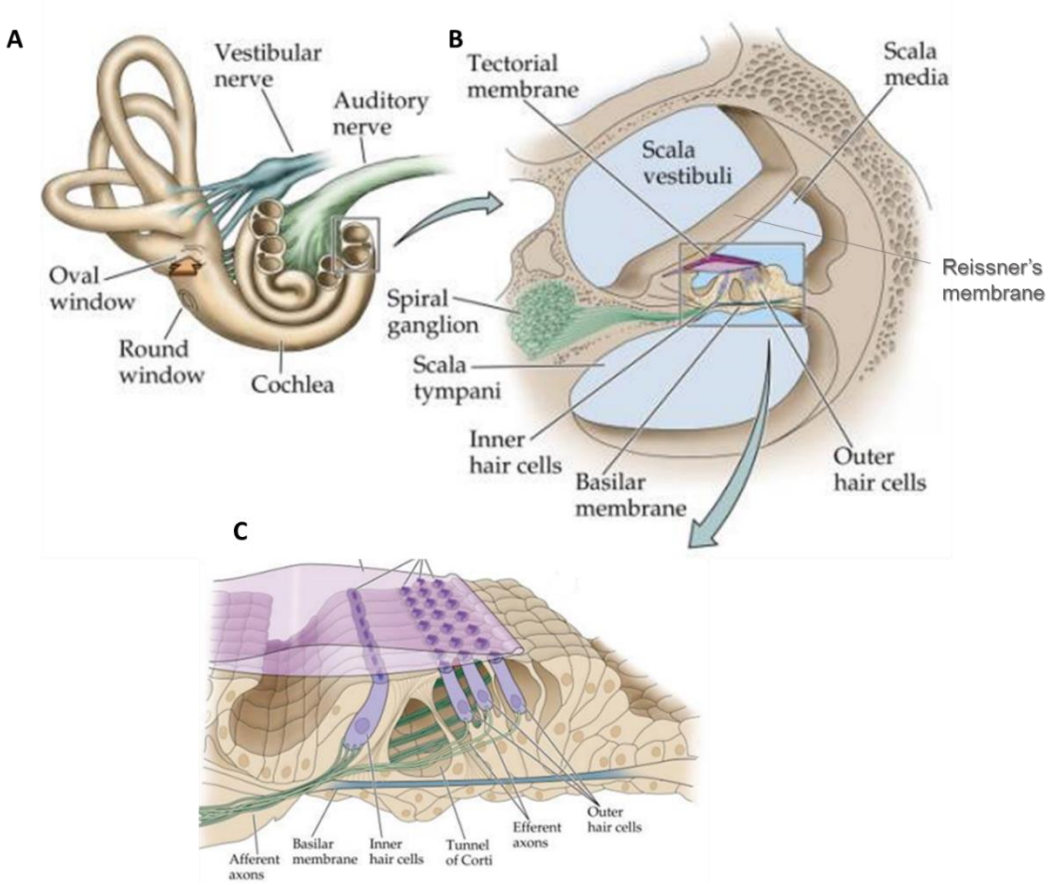

Figure 4- Inner ear structure. A- Inner ear; **B-** Cross section of cochlea; **C-** Organ of Corti structure (adapted from Purves, 2004).

1.4 Sensorineural hearing loss

In 2012 the World Health Organization (WHO) estimated that globally over 360 million people have disabling hearing loss (Wong and Ryan 2015). According to the Universal new born hearing screening in the United States of America, one in 1000 infants are born deaf and approximately one in 300 are affected with congenital hearing impairment (Mason and Herrmann 1998). In addition, one in 1000 children develop severe-to-profound hearing loss within the first two decades of life (Schrijver and Gardner 2006). Sensorineural hearing loss (SNHL) is a common sensory deficit being defined as the loss of hearing sensitivity caused by peripheral tissue damage and/or cell death in the cochlea. SNHL, in its non-syndromic form, can be the consequence of accumulation of many factors like free radical oxygen species, changes in calcium homeostasis and disturbed signalling pathways such as MAPK signalling pathways, which can culminate in cochlear cells apoptosis. Furthermore, infections that can lead to inflammation and immune responses may also be in the origin of SNHL (Wong and Ryan 2015).

1.5 Vestibular system

The vestibular system is a complex sensory system involving the communication between the peripheral vestibular apparatus, the ocular system, the postural muscles, the brainstem, the cerebellum and the cortex. With important sensory functions, vestibular system contributes to the perception of self-motion, head position and spatial orientation relative to gravity. It also assists important motor functions, helping to stabilize gaze, head and posture (Khan and Chang 2013; Yoder and Taube 2014).

The peripheral vestibular apparatus includes inner ear structures, cerebellum and somatic sensory cortices. The central portion of the system includes the vestibular nuclei, which make extensive connections with brainstem and cerebellar structures. The vestibular nuclei also directly innervate motor neurons controlling extraocular, cervical and postural muscles. This motor output is important to stabilization of gaze, head orientation and posture during movement. Balance, gaze stabilization during head movement and sense of orientation in space are all adversely affected if the system is damaged (Purves 2004; Pfeiffer et al. 2014).

The main peripheral component of the vestibular system is an elaborate set of interconnected chambers (the labyrinth) that has much in common, and is in fact continuous, with the cochlea. Once cochlea and labyrinth are derived from the same placode of the embryo it uses the same specialized set of sensory cells, the hair cells. These cells transduce physical motion into neural impulses. In the cochlea, the motion is due to airborne sounds whereas in the labyrinth, the motions transduced arise from head movements, inertial effects due to gravity and ground-borne vibrations. The labyrinth is buried deep in the temporal bone and consists of two otolith organs (the utricle and saccule) and three semi-circular canals (superior, posterior and horizontal). The utricle and saccule are specialized primarily to respond to linear accelerations of the head and static head position relative to the gravitational axis, whereas the semi-circular canals are specialized for responding to rotational accelerations of the head. The saccular macula is oriented vertically and the utricular macula horizontally. This morphological polarization allows that a tilt along the axis of the striola will excite the hair cells on one side while inhibiting the hair cells on the other side. The activity of the hair cells in the vestibular system is similar to their activity in cochlea, the deflection of the hair bundle is responsible to start the signal propagation to afferent neurons, but in this case it is not the basilar membrane that is responsible for the movement of the hair bundles but a fibrous structure, the otolithic membrane (Figure 5). The resulting shearing motion of the otolithic membrane displaces the hair bundles, which are embedded in the

lower, gelatinous surface of the membrane, inducing their response to mechanotransduction (Eatock and Songer 2011; Purves 2004).

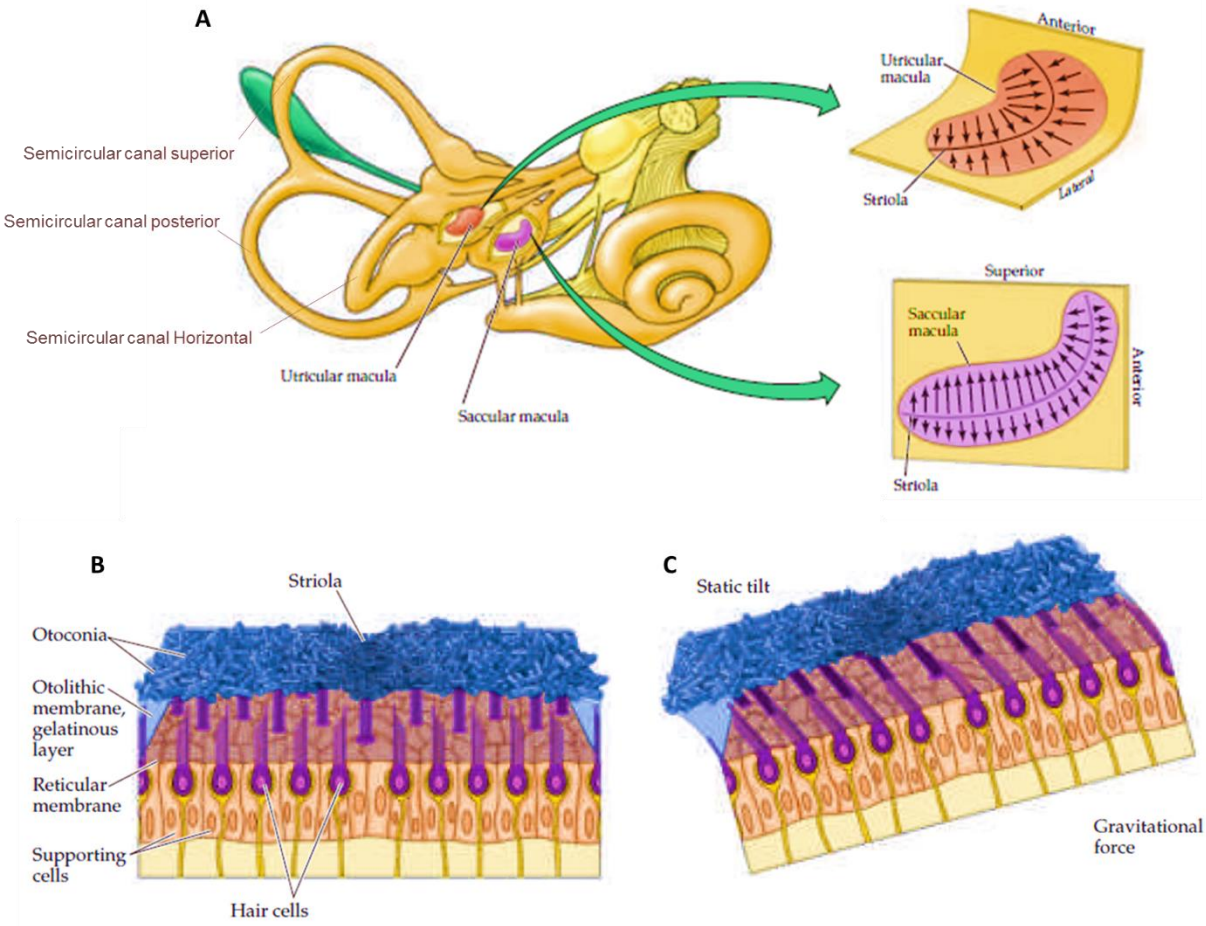

Figure 5- Morphological polarization of hair cells in the utricular and saccular maculae. **A-** the labyrinth and orientation of the utricular and saccular maculae in the head; arrows show orientation of the kinocilia **B-** Cross section of the utricular macula showing hair bundles projecting into the gelatinous layer when the head is level. **C-** Cross section of the utricular macula when the head is tilted. (adapted from Purves, 2004).

1.6 Usher syndrome

Usher Syndrome (USH) is a clinically heterogeneous disease characterized by the association of RP and SNLH, with or without vestibular dysfunction (Mathur and Yang 2015). Albrecht von Graefe, in 1858, reported for the first time the association of congenital deafness and progressive pigmentary retina dystrophy (Graefe 1858), but only in 1914 Charles Usher, a British ophthalmologist, defined the heritability of USH as an autosomal recessive disease and suggested the existence of at least two clinical subtypes of this syndrome based on the degree of hearing impairment, age of onset and progression of the visual loss (Usher

1935; Keats and Corey 2000). Later the prevalence of Usher Syndrome was estimated to be 3–6 per 100,000 (Steele-Stallard et al. 2013).

Distinguished by clinical features, there are three subtypes of USH: USH type 1 (USH1), USH type 2 (USH2) and USH type 3 (USH3). It is estimated that among all USH patients worldwide, 33-44% have USH1, 56-67% have USH2 and a very small percentage have USH3 (Petit 2001; Keats and Savas 2004; Vastinsalo et al. 2006).

USH1 patients, which show the most severe phenotype of the three subtypes, are clinically characterized by a congenital and bilateral SNHL that can be variable from severe to profound and present alterations in the vestibular function. In this subtype of USH, RP onset occurs during childhood. These patients usually do not develop a normal speech (Friedman et al. 2011).

In the USH2 patients the disease has a later onset when compared with the USH1 patients. Onset of USH2 occurs during or after puberty. Hearing impairment in this type of USH is moderate to severe with a normal vestibular function and RP usually occurring in the second decade of life (Dai et al. 2008).

USH3 patients can present a variable onset of progressive hearing loss, some have vestibular dysfunction, and a variable onset of progressive visual impairment (RP usually occurs in the second decade of life) (Millán et al. 2011).

In an animal model of the disease, the shaker-1 mice, an abnormal phagocytosis by RPE was described resulting in an abnormal renewal of photoreceptors outer segment. Additionally, it was also identified the mislocation of melanosomes in the animal RPE cells (Gibbs et al. 2003).

1.7 Genetics of USH

To date there are thirteen *loci* associated to USH. Nine of them are involved in USH1, three in USH2 and one in USH3. From these *loci*, ten genes have been identified with disease-causing mutations: *MYO7A* (*USH1B*) (Weil et al. 1995), *USH1C* (*USH1C*) (Verpy et al. 2000), *CDH23* (*USH1D*) (Bolz et al. 2001), *PCDH15* (*USH1F*) (Alagramam et al. 2001), *USH1G* (*USH1G*) (Weil et al. 2003) and *CIB2* (*USH1J*) (Riazuddin et al. 2012). For USH2, disease-causing mutations were identified in three genes: *USH2A* (*USH2A*) (Eudy et al. 1998), *GPR98* (*USH2C*) (Weston et al. 2004) and *WHRN* (*USH2D*) (Ebermann et al. 2007). Until now, only one gene was identified with disease-causing mutations for USH3, *CLRN1* (*USH3A*) (Joensuu et al. 2001). Table I reports the different USH associated *loci*.

Table I. USH *loci*

USH type	*Locus*	Location	Gene	Protein
USH1	*USH1B*	11q13.5	*MYO7A*	Myosin VIIa
	USH1C	11p14.3	*USH1C*	Harmonin
	USH1D	10q22.1	*CDH23*	Cadherin 23
	USH1E	21q21	n/a	n/a
	USH1F	10q21.1	*PCDH15*	Protocadherin 15
	USH1G	17q25.1	*USH1G*	SANS
	USH1H	15q22-q23	n/a	n/a
	USH1J	15q24	*CIB2*	CIB2
	USH1K	10p11.21-q21.1	n/a	n/a
USH2	*USH2A*	1q41	*USH2A*	Usherin
	USH2C	5q13	*GPR98*	VLGR1
	USH2D	9q32	*DFNB31*	Whirlin
USH3	*USH3A*	3q25	*CLRN1*	Clarin-1

Note: n/a- non associated.

1.8 *MYO7A*

MYO7A gene codes for myosin VIIa (myo7a) protein and is located on the long arm of chromosome 11 (11q13.5). Approximately 50% of USH1 families present mutations at *MYO7A* gene which is the most commonly mutated gene in this syndrome type followed by CDH23, PCDH15, USH1C, and USH1G (Liu et al. 2013) and CIB2 (Riazuddin et al. 2012). According to "The Universal Mutation database", until 2010, 1779 mutations were discovered (http://www.umd.be/MYO7A/). In human, myo7a transcript comprises 49 exons coding for a 2,215 amino acid protein and is expressed in several different tissues like retina, inner ear, testis, kidney, lung and olfactory epithelium, wherein retina has been the preferential tissue to study myo7a protein function. The myo7a protein contains three myosin typical domains: the N terminal head or motor, the neck or regulatory domain consisting of five IQ motifs and the tail which begins with a short coiled coil domain followed by two large repeats, each containing a MyTH4 (Myosin Tail Homology 4) and a FERM (Four-point-one, ezrin, radixin, moesin) domain, separated by a SH3 (SRC Homology 3) domain (Figure 6) (Lu et al. 2014).

Figure 6- Schematic representation of myosin VIIa structure.

The N-terminus motor-"head" is responsible for binding to actin filaments and for ATP hydrolysis-induced energy production. In the ADP-bound and nucleotide-free states, myosin motor binds strongly to actin, but if ATP or ADP-Pi are bound to myosin the affinity for actin is lower (Sweeney and Houdusse 2010).

The IQ motifs are responsible for mechanical force amplification, and a variable C-terminus tail for engaging with their specific targets. This modulation occurs due to calmodulin binding which induces different protein conformations depending on calcium levels. Considering this, the IQ motifs also regulate the activity of motor domain by actin-activated ATPase activity (Sakai et al. 2011; Sweeney and Houdusse 2010).

The SH3 domains are present in a variety of proteins associated with the organization of the actin cytoskeleton and with signal transduction. These domains are responsible for mediate protein-protein interactions through binding to proline rich stretches. In other myosins, like myosin I, the SH3 domains were described as essential for actin polymerization (Geli et al. 2000). In myo7a protein, the SH3 domain was associated to interactions with the C-terminus proline-rich region, a structure that is essential to myo7a roles since it may affect the orientation of the tail (Wang et al. 2007).

The MyTH4-Ferm are two domains involved in the interaction with several other proteins, conferring to myo7a protein important functions such as vesicles transport (El-Amraoui et al. 2002; Holt et al. 2007) and cell adhesion, namely by the association with tight junctions (Etournay et al. 2007). Myo7a protein was also associated with lysosomes but the reason for this association is not clear yet, even if it is obvious the association to intracellular transport events. The association with vesicles transports usually are made with rab and rab effectors as intermediate, such as rab27a and myrip in melanosomes transport as described further down (Soni et al. 2005).Munc13-4 is another rab effector which has been associated with intracellular vesicles transport, such as lysosomes (Bierings et al.2012).

In retina, several functions have been associated to myo7a protein and most of them are related with the correct photo transduction. One of these functions is opsin transport from the inner to the outer segment of photoreceptors through connecting cilium (Liu et al. 1999; Wolfrum and Schmitt 2000; Williams 2002). Furthermore, in RPE cells, which has been the preferential model to study myo7a functions, an important role in organelles (for exam-

ple, melanosomes) transport and phagosomes motility was revealed (Gibbs et al. 2003; Holt et al. 2007; Gibbs et al. 2010; Williams and Lopes 2011). The melanosomes transport by myo7a protein has been described to be made by a myo7a-myrip-rab27a protein complex. The interaction between myo7a and myrip was described to occur with the myo7a C-terminus FERM domain (El-Amraoui et al. 2002).

In the inner ear, myo7a protein was described as a generator of a large resting tension in the hair bundles (Gillespie 2002; Etournay et al. 2005). This protein has been involved in the sorting and/or targeting of harmonin to the hair bundle (Boëda et al. 2002; El-Amraoui and Petit 2005). Myo7a also interacts with vezatin, a cadherin-catenins complex associated protein that plays an important role in the establishment of strong cell-cell adhesions (Küssel-Andermann et al. 2000). This interaction allows to enhance the resilience of cochlear hair cells (Bahloul et al. 2009).

1.9 Background

Prior to the initiation of this study, a Targeted-Resequencing (TR) analysis of 9 of the known USH associated genes (*MYO7A*, *USH1C*, *CDH23*, *PCDH15*, *USH1G*, *USH2A*, *GPR98*, *WHRN* and *CLRN1*) was performed with the proband DNA sample in collaboration with Prof. Lee-Jun Wong from the Department of Molecular and Human Genetics, Baylor College of Medicine, Houston, TX, USA. This analysis allowed identifying 75 variants in 7 of the known USH associated genes and, after variants evaluation by using HGMD database, LOVD-USHbases, published articles, pathogenicity scored and categorized according to ACMG guidelines and published literature, and multiple *in silico* analytical tools, two novel heterozygous possible causing disease variants were identified in *MYO7A* gene, a c.3503+1delG and a c.5561dupT.

1.10 Objectives

The first aim of this work was to evaluate the family segregation of two possible compound heterozygous mutations in *MYO7A* gene (c.3503+1delG and c.5561dupT) found in a USH1 Portuguese patient. After this, it was also meant to determine the frequency of both variants in a healthy Portuguese population and perform *in silico* studies to evaluate the hypothesis that these variants probably are the primary cause of the phenotype in the USH1 patient.

This study also expected to confirm the presence of c.3503+1delG and c.5561dupT variant alleles in *MYO7A* gene transcripts using cDNA synthetized from nasal epithelium samples extracted total RNA, a tissue previously described as a good one to study variants in USH genes since it shows expression of almost all of them (Vaché et al. 2010).

Furthermore, this work intended to evaluate if c.5561dupT variant had any influence in the previously described interaction between myo7a protein and the rab-effector protein myrip. Finally, it is also aimed to evaluate if myo7a protein interacts with another rab-effector, the munc13-4 protein, and if any alteration of such interaction is disclosed in the presence of the c.5561dupT variant.

Chapter 2

Materials and Methods

2. Materials and Methods

2.1 Human subjects and samples

Clinical characterization of the USH patient was performed at the Otorhinolaryngology and Ophthalmology Departments of the Centro Hospitalar e Universitário de Coimbra, E.P.E. by Dr. João Carlos Ribeiro and Prof. Eduardo Silva. This study was approved by the Faculty of Medicine, University of Coimbra Ethics Committee, following the Tenets of the Declaration of Helsinki and a written consent for genetic testing was obtained from all the participants.

A three-generation Portuguese family with a total of 5 individuals (one affected, three normal and one deceased) (Figure 7) was investigated in this study. The 34 years old patient (III.1 in Figure 7) was diagnosed with deafness at 3 months of age, later described with vestibular dysfunction and, before puberty, presented RP with pigment spicules in the periphery. Considering all this, a clinical diagnostic of USH1 was made. Additionally, it is important to notice that the parents of the patient (II.1 and II.2 in Figure 7) are not consanguineous. A group of 250 samples from individuals without USH, 140 males and 110 females with an average age of 49.2±16.34 years and ranging from 12 to 84 years old, was also studied. Additionally, nasal epithelium samples were collected from the proband and two normal individuals without USH during surgery at the Otorhinolaryngology Department of the Cenro Hospitalar e Universitário de Coimbra, E.P.E. by Dr. João Carlos Ribeiro.

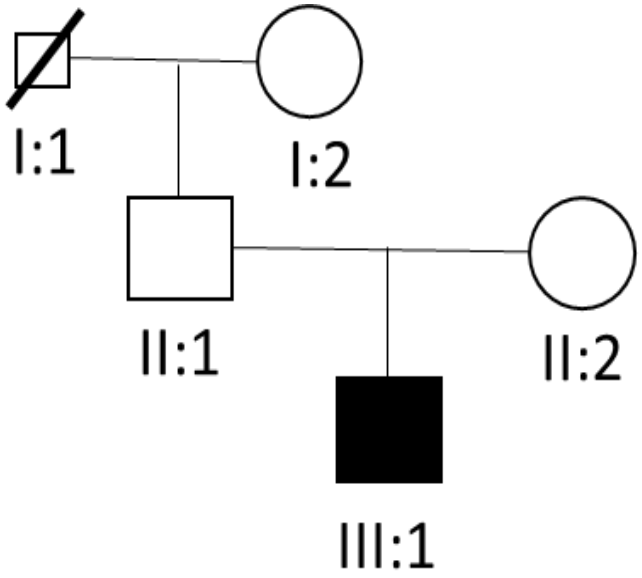

Figure 7- Proband's family pedigree. Squares represent males and circles represent females. The fill square represent proband. Crossed square represent deceased individual.

2.2 Methodologies

2.2.1 DNA extraction and quantification

Prior to the initiation of this study, peripheral blood was collected in EDTA Tubes (SARSTED) from the patient, the patient's relatives and the 250 normal individuals without USH, followed by DNA extraction using a standard phenol–chloroform method (Ausubel et al. 2003) in Prof. Manuela Grazina Biochemical Genetics Laboratory, Center for Neurosciences and Cellular Biology of Coimbra. The extracted DNA was quantified by spectrophotometry at optical density of 260nm and 280 nm using the NanoDrop™ 1000 (Thermo Fisher Scientific, Inc.) and the GeneQuant™ II (Pharmacia Biotech). Protein-free DNA samples give a ratio of 1.75-2.0 reading at 260 nm/280 nm.

2.2.2 Polymerase Chain Reaction (PCR) for DNA samples

MYO7A gene exons 27, 30, 35, 36, and 40 and adjacent regions were amplified by PCR using the Primers designed with Primer3 software (http://bioinfo.ut.ee/primer3-0.4.0/primer3/) (Table II) and the *MYO7A* gene reference sequence obtained from NCBI database (http://www.ncbi.nlm.nih.gov/gene/). The PCRs were run on a Veriti® Thermal Cycler (Applied Biosystems) and the PCR reactions were performed using 50-100ng of genomic DNA mixed with 1X Taq Buffer 10X (with $(NH_4)_2SO_4$) (Fermentas), 0.2µM of Forward and Reverse Primers (Sigma-Aldrich), 1.5-2.5mM $MgCl_2$ (Fermentas), 0.2mM dNTPs (5PRIME), 1U Taq Polymerase (Fermentas) and RNAse/DNAse free Water (AccuGENE) to a final volume of 10µl. The reaction mixtures were subjected to a specific PCR program with an initial denaturation step of 5 minute (min) at 95°C followed by 35 cycles, each with denaturation at 95°C for 30 seconds (sec), annealing at 58-62°C for 30 sec, and extension for 1 min at 72°C, with a final elongation step of 10 min at 72°C.

Table II. Primers used for amplification of MYO7A gene exons 27, 30, 35, 36 and 40

Exon	Primer sequence (5'-3')	
Exon 27	Fw	AGGAGGTGGCCAGAGGAG
	Rev	GACAGAGGCACCACTCAGC
Exon 30	Fw	CAGTCCTGACCTCTCAGC
	Rev	GAGGACACAGGACTGAGGACA
Exon 35	Fw	ACAGGCAAAGGAGAAGTAGGC
	Rev	CAAGATCCTAGCAGCCTTGAG
Exon 36	Fw	AGTAGCCCACTCTGGTGATG
	Rev	GGTGATACACTTCTCTCCAATC
Exon 40	Fw	GTTGCATCTGGCTGTCAGG
	Rev	ACAAGTGCCCTCGGAGAGT

2.2.3 Electrophoresis

PCR products underwent an electrophoresis on an agarose gel containing 1% agarose SeaKem LE (Lonza) and 1% ethidium bromide (Acros/Fisher Bioreagents) in 1x Tris Borate EDTA (TBE) solution (National diagnostics). The products with a Loading Buffer (Bio-Rad) migrated under an electric current of 200 volts for 15 minutes (min). A *NZY DNA Ladder* VI (NZYTech) was also used to estimate the size of the fragments and respective quantification by comparison with the Molecular Weight Marker. The fragments were visualized through UV light in the ChemiDoc™ XRS System and respective System with Image Lab™ Software (Bio-Rad).

2.2.4 Restriction Fragment Length Polymorphism (RFLP)

PCR products for exon 27 were digested with BsaW I (New England BioLabs) restriction endonuclease incubating at 60°C overnight. The RFLP reaction was performed in a final volume of 15 µl containing 5 µl of PCR product, 1.5 µl of NEBuffer 4, 0.15 µl of BSA, 1 U of BsaW I enzyme and RNAse/DNAse free Water (AccuGENE) up to the final volume. Digested PCR products mixed with Loading Buffer (Bio-Rad) were submitted to an electrophoresis under an electric current of 200 volts for 20 min on an agarose gel

containing 2% agarose SeaKem LE (Lonza) and 1% ethidium bromide (Acros/Fisher Bioreagents) in 1x TBE solution (National diagnostics). A NZY DNA Ladder VI (NZYTech) was used as a Molecular Weight Marker. The fragments were visualized through UV light in the ChemiDoc™ XRS System and respective System with Image Lab™ Software (Bio-Rad).

PCR products for exon 40 were digested with Eco72 I (New England BioLabs) restriction endonuclease incubating at 37°C during 1hour (h). The RFLP reaction was performed in a final volume of 15 µl containing 2 µl of PCR product, 1.5 µl of Tango Buffer, 1 U of Eco72 I enzyme and RNAse/DNAse free Water (AccuGENE) up to the final volume. Digested PCR products mixed with Loading Buffer (Bio-Rad) were submitted to an electrophoresis under an electric current of 200 volts for 15 min on an agarose gel containing 1% agarose SeaKem LE (Lonza) and 1% ethidium bromide (Acros/Fisher Bioreagents) in 1x TBE solution (National diagnostics). A NZY DNA Ladder VI (NZYTech) was used as a Molecular Weight Marker. The fragments were visualized through UV light in the ChemiDoc™ XRS System and respective System with Image Lab™ Software (Bio-Rad).

2.2.5 Purification of PCR products for Sequencing reaction

The amplified PCR products for *MYO7A* gene exons 27, 30, 35, 36 and 40, later used for Sequencing reaction, were purified using 1µl of ExoSAP-IT® (USB)/4µl of amplified PCR product, incubated at 37°C for 1h followed by 15 min at 75°C on a Veriti® Thermal Cycler (Applied Biosystems).

2.2.6 Sequencing reaction

Sequencing reactions were performed with 10ng of PCR products, 1X BigDye® Terminator 5X Sequencing Buffer (Applied Biosystems), 0.16µM of Forward or Reverse Primer (Sigma-Aldrich), BigDye® Terminator v3.1 according to manufacturer recommendations (Applied Biosystems) and RNAse/DNAse free Water (AccuGENE) for a final volume of 10µl. The Primers used were the same as for PCR products amplification (Table I). Sequencing reaction was run on a Veriti® Thermal Cycler (Applied Biosystems) using the following conditions: an initial denaturation step of 2 min at 96°C followed by 25 cycles each of a denaturation at 96°C for 5 sec, annealing at 58-62°C for 10 sec, followed by one last step of elongation at 60°C for 4 min.

2.2.7 Purification of Sequencing reaction products

A total of 8µl of RNAse/DNAse free Water (AccuGENE) and 32µl of 95% ethanol (Merck) were independently added to each Sequencing reaction product followed by capping and inversion of the plate for mixing the reagents. After 15 min of rest at room temperature (RT), the solution was subjected to a centrifugation at 2500 RCF for 30 min). The supernatants were discarded in a paper towel and the samples were washed with 75µl 70% ethanol (Merck). The plate was capped and inverted a few times, followed by centrifugation at 2000 RCF during 10 min. The supernatants were discarded as previously and the inverted plate on a paper towel was centrifuged at 700 RCF for 1 min. Purified Sequencing reaction products were resuspended with 10 µl of HiDi™ (Applied Biosystems) and denatured at 96°C for 5 min on a Veriti® Thermal Cycler (Applied Biosystems) previously to be analyzed by Capillary electrophoresis.

2.2.8 Capillary electrophoresis

Automated capillary DNA Sequencing was performed on a Genetic Analyzer 3130 (Applied Biosystems) equipment. DNA sequencing data obtained was analyzed using Sequencing Analysis Software v.5.4® (Applied Biosystems) that allowed the identification of *MYO7A* gene variants by comparison with gene reference sequence (http://www.ncbi.nlm.nih.gov/sites/entrez).

2.2.9 *In silico* analysis

The evolutionary conservation study, both in nucleotides and in amino acids sequences, included primate species that have several similarities with humans (*Homo sapiens*), such as Chimpanzee (*Pan troglodytes*), Gorilla (*Gorilla gorilla*), Macaque (*Macaca mulatta*) and Orangutan (*Pongo abelli*), and non-primates species such as Mouse (*Mus musculus*), Rat (*Rattus norvegicus*), Zebrafish (*Danio rerio*), Fruitfly (*Drosophila Melanogaster) and* Nematode *(Caenorhabditis elegans)*. The www.ensembl.org was the genome database used for all necessary species sequences.

The splicing site alteration prediction was performed using *MYO7A* gene exon 27 and adjacent nucleotide sequence from www.ensembl.organd the free online software http://www.fruitfly.org/seq_tools/splice.html by comparing the wild type (wt) with the c.3501+1delG variant sequences.

2.2.10 RNA extraction, quantification and integrity evaluation

The total RNA extractions from patient's and the two normal individuals without USH nasal epithelium samples were performed with RNeasy minikit® (QIAGEN®) including an additional step with RNAse-Free DNAse Set (QIAGEN®), after homogenization of nasal epithelium samples with the TissueLyser II (QIAGEN®) according to manufacturer recommendations. Total RNA samples quantification and integrity evaluation based on the RNA integrity number (RIN), was determined with the Bioanalyzer (Agilent Technologies) according to manufacturer recommendations.

2.2.11 Reverse Transcriptase (RT)-PCR

The total RNA samples were used to synthetize cDNA by RT-PCR with the High-Capacity cDNA Reverse Transcription Kit (Life Technologies) according to manufacturer recommendations and using a Veriti® Thermal Cycler (Applied Biosystems).

2.2.12 PCR for cDNA samples

B2M (used to control the presence of cDNA) and *MYO7A* Exon 40 intronic primers (used to control the absence of genomic DNA) (Table III) were used to control cDNA quality. Primers were designed with Primer3 software (http://bioinfo.ut.ee/primer3-0.4.0/primer3/) and the reference *B2M* transcript sequence obtained from NCBI database (http://www.ncbi.nlm.nih.gov/gene/). The PCR technique was performed on a Veriti® Thermal Cycler (Applied Biosystems)with 50ng of cDNA mixed with the following reagents: 1X Taq Buffer 10X (with (NH4)2SO4) (Fermentas), 0.2µM of Forward and Reverse Primers (Sigma-Aldrich), 1.5mM $MgCl_2$ (Fermentas), 0.2mM dNTPs (5PRIME), 1U Taq Polymerase (Fermentas) and RNAse/DNAse free water (AccuGENE) to a final volume of 10µl. The

reaction mixtures were subjected to a specific PCR program with an initial denaturation step of 5min at 95°C followed by 35 cycles, each with denaturation at 95°C for 30sec, annealing at 60°C for 30 sec, and extension for 1 min at 72°C, with a final elongation step of 10 min at 72°C.

Regions surrounding both mutations from *MYO7A* transcript were amplified by Polymerase Chain Reaction (PCR) technique using the Primers designed with Primer3 software (http://bioinfo.ut.ee/primer3-0.4.0/primer3/) (Table III) and the reference *MYO7A* transcript sequence obtained from NCBI database (http://www.ncbi.nlm.nih.gov/gene/). The PCR technique was performed on a Veriti® Thermal Cycler (Applied Biosystems). The PCR reactions were performed using 50-400 ng of cDNA mixed with the following reagents: 1X Taq Buffer 10X (with $(NH_4)_2SO_4$) (Fermentas), 0.2µM of Forward and Reverse Primers (Sigma-Aldrich), 1.5-2.5mM $MgCl_2$ (Fermentas), 0,2mM dNTPs (5PRIME), 1U Taq Polymerase (Fermentas) and RNAse/DNAse free water (AccuGENE) to a final volume of 10µl. The reaction mixtures were subjected to a specific PCR program with an initial denaturation step of 5min at 95°C followed by 35 cycles, each with denaturation at 95°C for 30sec, annealing at 60°C for 30 sec, and extension for 1 min at 72°C, with a final elongation step of 10 min at 72°C. PCR reactions were performed with a negative control of PCR (without cDNA sample) and a negative control of RT-PCR (product of RT-PCR, performed without RNA sample).

Table III. Primers used for cDNA samples amplification

target to amplify:	**Primer sequence (5' - 3')**	
c.3501+1delG	Fw	CTCACAGCGGCGGTGACCAAG
	Rev	CGTCCTCCTTCTCACACC
c.5561dupT	Fw	CCCTGGTCACCATGACTCC
	Rev	CACAATTCCGTCCTTGATGG
B2M	Fw	GGCTATCCAGCGTACTCCAA
	Rev	GAGAATTTGGAATTCATCCAATC
Intronic primers surrounding Exon 40	Fw	GTTGCATCTGGCTGTCAGG
	Rev	ACAAGTGCCCTCGGAGAGT

2.2.13 Electroforesis of cDNA samples PCR products

PCR products underwent an electrophoresis performed according to section 2.2.4.

2.2.14 Purification of cDNA samples PCR products for Sequencing reaction

The amplified cDNA samples PCR products later used for Sequencing reaction were purified according to section 2.2.6.

2.2.15 cDNA samples PCR products Sequencing reaction

cDNA samples PCR products Sequencing reactions were performed according to section 2.2.7.

2.2.16 Purification of Sequencing reaction products obtained from cDNA samples

Sequencing reaction products were purified with Illustra Sephadex G-50 DNA Grade F, 100 g (GE Healthcare Life Sciences) according to manufacturer recommendations. 2µl of purified Sequencing reaction products were diluted with HiDi™ (Applied Biosystems) to a final volume of 10µl of and denatured at 96°C for 5 min on a Veriti® Thermal Cycler (Applied Biosystems), previously to be analyzed by Capillary electrophoresis.

2.2.17 cDNA samples Sequencing reaction products Capillary electrophoresis

Automated Capillary cDNA samples Sequencing reaction products were performed according to section 2.2.8.

2.2.18 cDNA samples PCR products-RFLP

cDNA samples PCR products for exon 40 were digested with Eco72I (New England BioLabs) according to section 2.2.4.

2.2.19 Site Directed Mutagenesis

A pENTR GFP C2 Myo7a F3 wt plasmid (provided by José Ramalho PhD - CEDOC Chronic Diseases Faculdade de Ciências Médicas, Universidade Nova de Lisboa) was used as a template to create a pENTR GFP C2 Myo7a F3 mut by site directed mutagenesis. PCR technique using the Primers designed with Primer3 software (http://bioinfo.ut.ee/primer3-0.4.0/primer3/) (Table IV), aimed to amplify the plasmid region containing the GFP-*MYO7A*(F3) and cause the mutation *MYO7A* c.5561dupT. The PCR technique was performed on a Veriti® Thermal Cycler (Applied Biosystems). The PCR reactions were performed using 1:100 diluted plasmid DNA template mixed with the following reagents: 1X iProof HF Buffer 5X (with 7.5mM $MgCl_2$) (Bio-Rad), 0.5µM of Forward and Reverse Primers (Sigma-Aldrich), 0.2mM dNTPs (5PRIME), 0.02U/µl iProof™ High-Fidelity DNA Polymerase (Bio-Rad), 3% DMSO (Bio-Rad) and RNAse/DNAse free water (AccuGENE) to a final volume of 50µl. The reaction mixtures were subjected to a specific PCR program with an initial denaturation step of 2min at 98°C followed by 32 cycles, each with denaturation at 98°C for 20sec, annealing at 58°C for 20sec, and extension for 1min and 30sec at 72°C, with a final elongation step of 10min at 72°C.

After that, PCR products underwent an electrophoresis on an agarose gel containing 1.5% agarose SeaKem LE (Lonza) and 1% ethidium bromide (Acros/Fisher Bioreagents) in 1x TBE solution (National diagnostics). The products with a Loading Buffer (Bio-Rad) migrated under an electric current of 90mA for 15min. A NZY DNA Ladder VI (NZYTech) was also used to estimate the size of the fragments. The fragments were visualized through UV light in the ChemiDoc™ XRS System and respective System with Image Lab™ Software (Bio-Rad). The fragments were extracted from gel with QIAEX II Gel Extraction Kit (Qiagen) according to manufacturer recommendations.

The extracted DNA products were merged by PCR. PCR technique using the Primers designed with Primer3 software (http://bioinfo.ut.ee/primer3-0.4.0/primer3/) (Table IV). The PCR technique was performed on a Veriti® Thermal Cycler (Applied Biosystems). The PCR reactions were performed using 1:75 diluted DNA template mixed with the following

reagents: 1X iProof HF Buffer 5X (with 7.5mM $MgCl_2$) (Bio-Rad), 0.2mM dNTPs (5PRIME), 0.02U/µl iProof™ High-Fidelity DNA Polymerase (Bio-Rad), 3% DMSO (Bio-Rad) and RNAse/DNAse free water (AccuGENE) to a final volume of 50µl. The reaction mixture was subjected to a specific PCR program with an initial denaturation step of 2min at 98°C followed by 5 cycles, each with denaturation at 98°C for 20sec, annealing at 58°C for 20sec, and extension for 2min and 30sec at 72°C, with a final elongation step of 10min at 72°C. After that, 0,5µM of Forward and Reverse Primers (Sigma-Aldrich) were added and the reaction mixture was subjected to a specific PCR program with an initial denaturation step of 2min at 98°C followed by 32 cycles, each with denaturation at 98°C for 20sec, annealing at 58°C for 20sec, and extension for 2min and 30sec at 72°C, with a final elongation step of 10min at 72°C.

PCR products underwent an electrophoresis on an agarose gel containing 1.5% agarose SeaKem LE (Lonza) and 1% ethidium bromide (Acros/Fisher Bioreagents) in 1x TBE solution (National diagnostics). The products with a Loading Buffer (Bio-Rad) migrated under an electric current of 90 mA for 15min. A NZY DNA Ladder VI (NZYTech) was also used to estimate the size of the fragments. The fragments were visualized through UV light in the ChemiDoc™ XRS System and respective System with Image Lab™ Software (Bio-Rad). The fragments were extracted from gel with QIAEX II Gel Extraction Kit (Qiagen) according to manufacturer recommendations.

Extraction product and template plasmid were digested with EcoR I and Sma I (Invitrogen) restriction enzymes according to manufacturer recommendations, and PCR products underwent an electrophoresis on an agarose gel and gel extraction as previously described in this section. Both fragments were linked with T4 DNA Ligase (Takara) in an overnight incubation at 37°C.

After that, *Escherichia coli* (*E. coli*) DH5α bacteria were transform with plasmid by thermal shock, wherein *E. coli* and plasmid were preserved in ice during 30 min and immediately after, placed at 42°C during 30min. After that the bacteria were grown in Luria-Bertani (LB) medium during 1h. Posteriorly, *E. coli* were seeded in a agar plate and colonies were sequenced to select the ideal clones (as described in section 2.2.6.).

Table IV. Primers used for Site Directed Mutagenesis

Primer	Primer sequence (5' - 3')	
***MYO7A* c.5561dupT**	Sense	CACGTTGCAGCGCTTCTT
	Anti-sense	AGGAAGCGCTGCAACGTG
pENTR *GFP* C2	Fw	TGAAACCTTTTACAGCATTGTTGAGGCGG
	Rev	CCACATTTGTAGAGGTTTTACTTGC

2.2.20 Cell culture

Human Embryonic Kidney 293a cell line (HEK-293a) was maintained in Dulbecco's Modified Eagle Medium (DMEM) (Life Technologies), supplemented with 10% Fetal bovine serum (FBS) (Gibco®-Life technologies), 1% Penicillin/Streptomycin (100 U/mL/100µg/mL) (Gibco®-Life technologies) and 1% GlutaMAX (Life Technologies), at 37°C under 5% CO_2.

2.2.21 HEK-293a transfection

Aiming to have a 70% confluent cell culture at the time of transfection, HEK-293a cells were seeded in 35 x 10mm plates one day before. For each transfection sample, 2ng plasmid DNA was diluted in 50µl Opti-MEM I Reduced Serum Media (Life Technologies). Subsequently, 1µl Lipofectamine 2000 (Life Technologies) transfection reagent was diluted in 50µl Opti-MEM medium and incubated for 5min at RT. After this incubation, diluted plasmid DNA (Table V) and Lipofectamine were mixed and further incubated for additional 20min. When incubation time was finished, DNA/Lipofectamine complexes were added to the normal cell culture medium. The cells were incubated at 37°C, under 5% CO_2, for 24h prior to performing the Immunoprecipitation (IP) and Immunofluorescence assays.

After incubation with plasmid DNA, cells were rinsed twice with phosphate buffered saline solution (PBS) (Sigma-Aldrich®), collected immediately in 50µL of 4x Laemmli Buffer (250mM Tris-HCl (pH 6.8), 35% (v/v) glycerol, 20% (v/v) β-mercaptoethanol, 8% (m/v) SDS, 0.03% (m/v) bromophenol blue) and boiled for 5min at 95°C.

Table V. Vectors used to transfect HEK293a cells

Protein	Tag	Plasmid
Myo7a C-terminus wt	GFP	pENTR GFP C2 Myo7a Fragment3
Myo7a C-terminus mut	GFP	pENTR GFP C2 Myo7a Fragment3 c.5561dupT
Myrip full length	Myc	pCMV myc MyRIP
Munc13-4 full length	V5	pENTR V5 C3 Munc13-4

2.2.22 Western blot

For Western Blot (WB) analysis, proteins were separated by electrophoresis on a 10-15% polyacrylamide (NZYTech) gel containing sodium dodecyl sulfate (Bio-Rad) (SDS-PAGE). After electrophoresis, proteins were electro-transferred to nitrocellulose membranes followed by membranes blocking with 5% (m/v) nonfat milk in Tris-buffered saline (TBS) (50 mM Tris (pH 7.6), 150 mM NaCl)-Tween-20 0.01% (v/v) (TBS-T), for at least 30min under agitation at RT. Membranes were incubated with primary antibodies diluted in TBS-T supplemented with 5% non-fat milk overnight at 4°C and subsequently incubated with horseradish peroxidase (HRP) conjugated secondary antibodies with agitation for 1h at RT. The immunoreactive bands were visualized with enhanced chemiluminescence (ECL) reagent, revealed by scanning blots using a VersaDoc (Bio-Rad Life Science) imaging system.

2.2.23 IP assays

After transfection, HEK-293 cells cultured at 60 x 15mm plates were washed twice in ice-cold PBS, scraped off the dishes and lysed in 100µl Radioimmunoprecipitation assay (RIPA) buffer (150mM NaCl, 50mM Tris-HCl, 1% NP-40 (nonyl phenoxypolyethoxylethanol) and 0.1% SDS, pH 7.5) containing protease and phosphatase inhibitors [protease inhibitor cocktail (Roche), 2mM phenylmethanesulfonyl fluoride (PMSF) (Sigma-Aldrich®), 10mM iodoacetamide (Sigma-Aldrich®) and 2mM sodium ortovanadate (Sigma-Aldrich ®)]. The samples were centrifuged at 16000 RCF for 10min at 4°C, and 5% of the total amount of protein in the lysates was denatured (inputs), while the remaining lysates was used for IP.

Briefly, supernatants were incubated with 10µg of goat polyclonal antibodies directed against GFP protein. Supernatants without antibodies were used as negative controls. Incubation with gentle agitation was performed for 3h at 4°C, followed by adding 40µg of protein G-Sepharose (GE Healhcare Biosciences) to the samples and incubation for 1.5h at 4°C. The samples were then centrifuged at 2300 RCF for 3min and the protein G-Sepharose sediments washed twice in RIPA buffer and once with PBS. Then, the samples were eluted with 3x Laemmli buffer and denatured at 95°C for 5min. WB analysis of the eluates was performed as already described.

Table VI. List of primary and secondary antibodies used for WB and confocal microscopy analysis

Antibody	Host/ Clonality	Clone/ Cat#	Application	Dilution	Company
Anti-GFP	goat	AB0020	IP/WB	1:2500	SICGEN
Anti-myc	goat	AB0127-200	WB/IF	1:1000	SICGEN
Anti- V5	rabbit	PAI-993	WB/IF	1:1000	Invitrogen
Anti-goat IgG- HRP	rabbit	61-1620	WB	1:5000	Life Technologies
Anti-rabbit IgG-HRP	goat	656120#	WB	1:10000	Bio-Rad
alexa 568 anti-goat	rabbit	A-11004	IF	1:200	Molecular Probes, Life Technologies
alexa 568 anti-rabbit	goat	A-11011	IF	1:200	Molecular Probes, Life Technologies

Note: WB- Western blot; IP- Immunoprecipitation; IF- Immunofluorescence.

2.2.24. Immunofluorescence assay

HEK293a cells grown on glass coverslips were fixed with 4% paraformaldehyde in PBS. Then, the samples were washed with PBS, permeabilized with 0.2% v/v Triton X-100 (MERK) in PBS and blocked with goat serum (1:10) for 20min prior to incubation with primary antibodies. Incubation with antibodies proceeded for 1h at RT. The samples were then washed three times with PBS before incubation with the secondary antibody for 1h at RT. The samples were rinsed in PBS and mounted with MOWIOL 4-88 Reagent (Calbiochem). Nuclei were stained with DAPI (Sigma-Aldrich®). All solutions were made in 0.2% w/v BSA (Sigma) containing 0.02% sodium azide (Sigma-Aldrich®) in PBS. Images were collected by confocal microscopy using a Zeiss LSM 710 (Zeiss).

Chapter 3

Results

3. Results

3.1 Genetic studies

PCR-Sequencing reactions of patient's *MYO7A* gene exons 27 and 40, and the adjacent regions, allowed identifying variants c.3503+1delG (Figure 8A) and c.5561dupT (Figure 8B), respectively, confirming previous TR results obtained through the collaboration with Prof. Lee-Jun Wong from the Department of Molecular and Human Genetics, Baylor College of Medicine, Houston, TX, USA. Additionally, a novel 22 nucleotide deletion was found in intron 27, the c.3503+12_33del (Figure 9). Further analysis of patient's relatives allowed genotyping this novel variant. Moreover, aiming to determine if the novel variants segregated in proband's family, genotyping of c.3503+1delG, c.5561dupT, c.3503+12_33del and three other variants (rs2276285, rs7927472 and rs2276288) previously identified in patient's DNA sample in heterozygosity by TR was performed and the results can be seen in Figure 10. While analyzing *MYO7A* gene exon 36, a seventh heterozygous variant (rs12292189) was found in patient's DNA sample and further genotyped in his family relatives. The sequencing results for c.3503+1delG and c.5561dupT variants in patient and his relatives' DNA samples were also confirmed by PCR-RFLP with restriction enzymes BsaW I and Eco72 I, respectively (Figure 11).

Aiming to evaluate the genotypic and allelic frequencies of c.3503+1delG and c.5561dupT variants in the Portuguese population, 250 samples from individuals without USH were analysed with the same PCR-RFLP procedure and all of them displayed a homozygous wild type genotype.

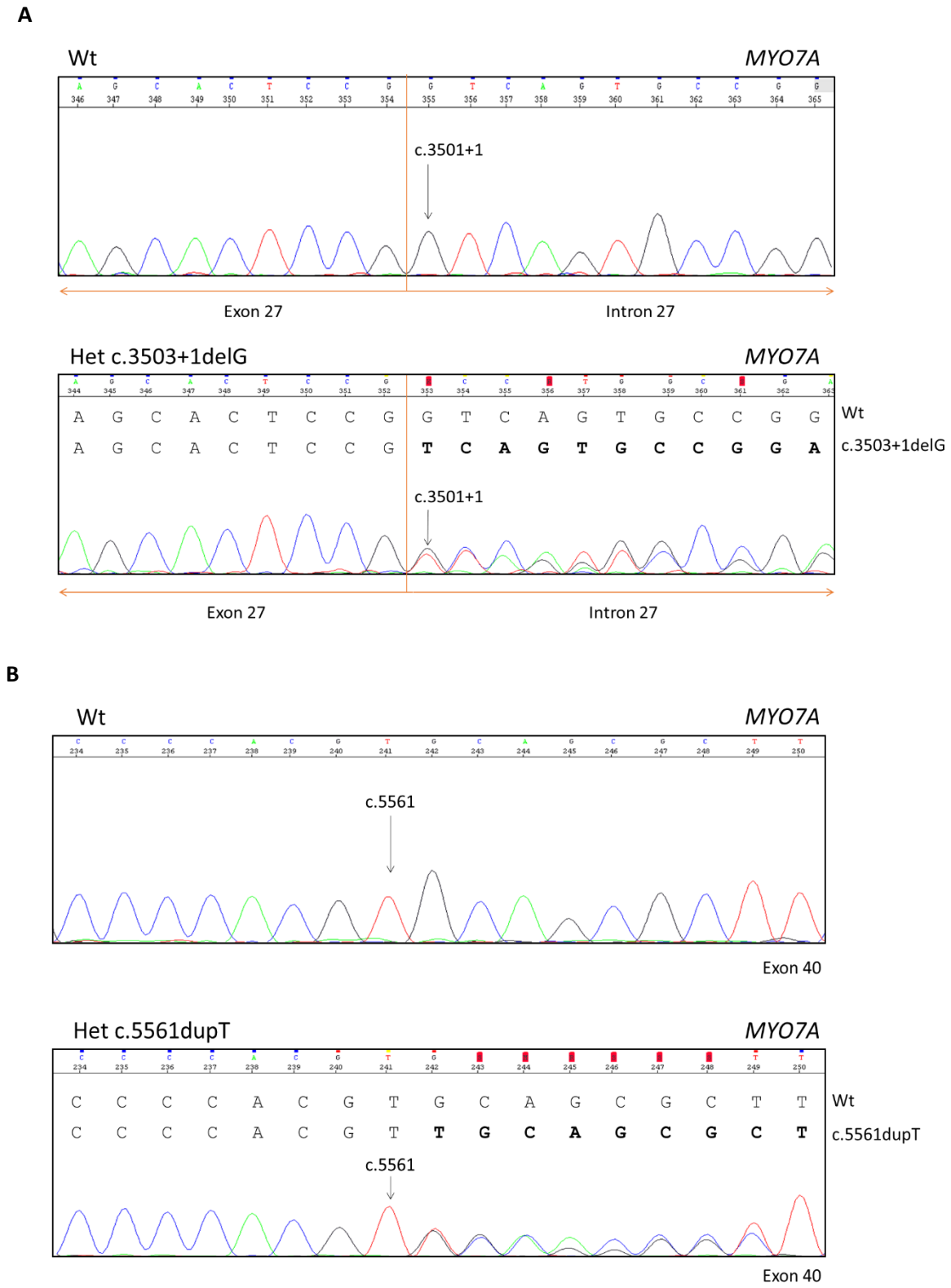

Figure 8- Electropherograms of the *MYO7A* gene c.3503+1delG and c.5561dupT surrounding regions. A- In the top can be seen a homozygous wt sequence and in the bottom a heterozygous c.3503+1delG. **B**- In the top can be seen a homozygous wt sequence and in the bottom a heterozygous c.5561dupT.

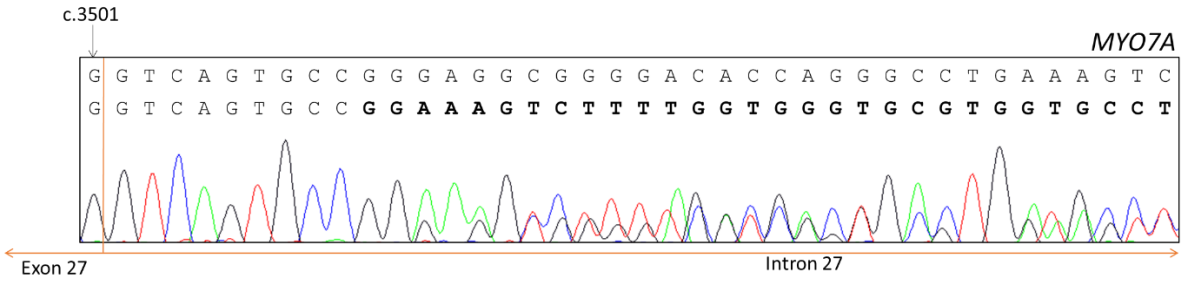

Figure 9- Electropherograms of the *MYO7A* gene c.3503+12_33del surrounding regions.

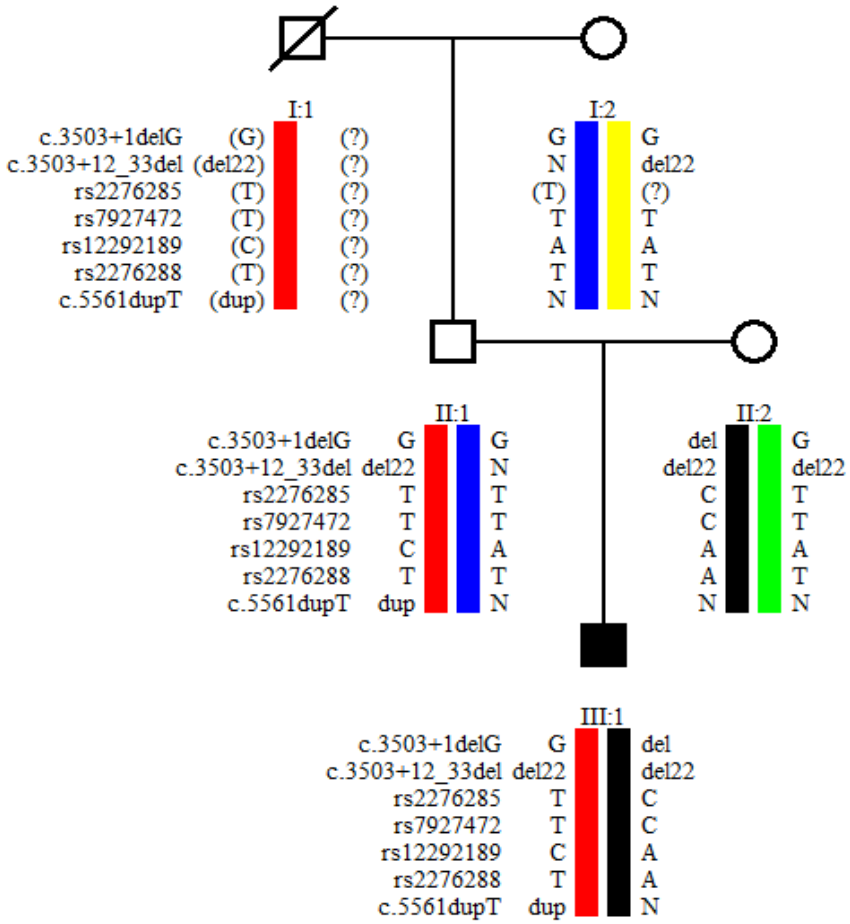

Figure 10- Representation of proband's family pedigree with haplotypes of the studied *MYO7A* gene variants. Note that proband carries all variants in heterozygosity with the exception of c.3503+12_33del which is in homozygosity.

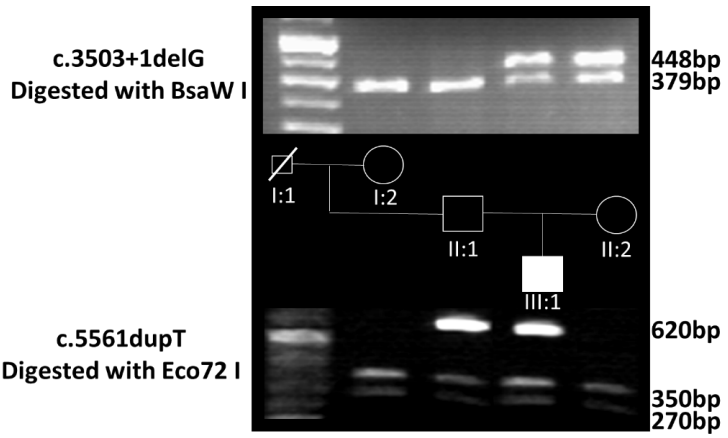

Figure 11- Representation of proband's family pedigree with electrophoresis photographs of PCR-RFLP analysis for *MYO7A* gene nucleotides c.3503+1 (top) and c.5561 (bottom). In the top, after digestion of the 448bp amplicon with BsaW I, individuals I:2 and II:1 present two bands with 379bp and 69bp (not shown) corresponding to a G/G genotype, while individuals II:2 and III:1 present three bands of 448bp, 379bp and 69bp (smallest band not shown) corresponding to the heterozygous G/del genotype. In the bottom, after digestion of the 620bp amplicon with Eco72 I, individuals I:2 and II:2 present two bands of 350bp and 270bp corresponding to N/N genotype, while individuals II:1 and III:1 present three bands of 620bp, 350bp and 270bp corresponding to the heterozygous N/dup genotype.

3.2 *In silico* analyses

Bioinformatics analysis is a useful tool to predict sequence variations pathogenicity. In this study, the *in silico* analyses were performed for *MYO7A* c.3503+1delG and c.5561dupT genetic variants.

3.2.1 Evolutionary conservation

Evolutionary conservation study was performed for the two possible USH1-causing disease variants using a primates and non-primates groups. In Figure 12 are represented the results of evolutionary conservation study for *MYO7A* c.3503+1delG variant. All mammals species present a high similarity in the nucleotide sequence surrounding c.3503+1, while the non-mammals species show a lower similarity. In Figure 13 are represented the results of evolutionary conservation study for *MYO7A* c.5561dupT variant. All vertebrates species present a high similarity in the nucleotide and amino acid sequences surrounding c.5561, while the *D. melanogaster* and *C.elegans* show a lower similarity.

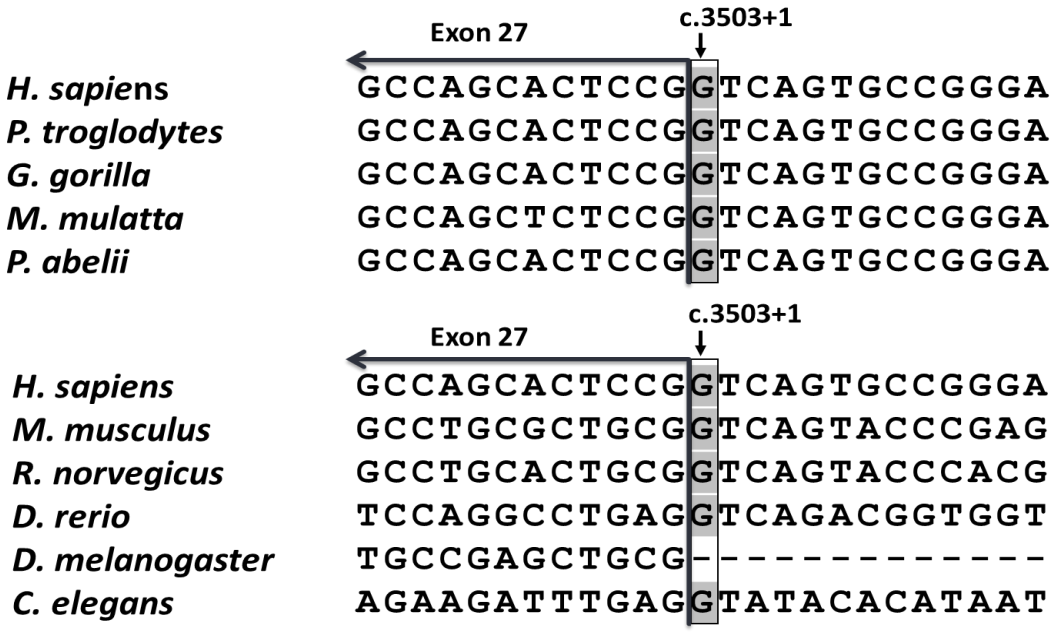

Figure 12- Nucleotide evolutionary conservation study for *MYO7A* gene c.3503+1delG variant. A- Nucleotide evolutionary conservation of *MYO7A* gene c.3503+1delG variant in primates species. **B-** Nucleotide evolutionary conservation of *MYO7A* gene c.3503+1delG variant in non-primates species.

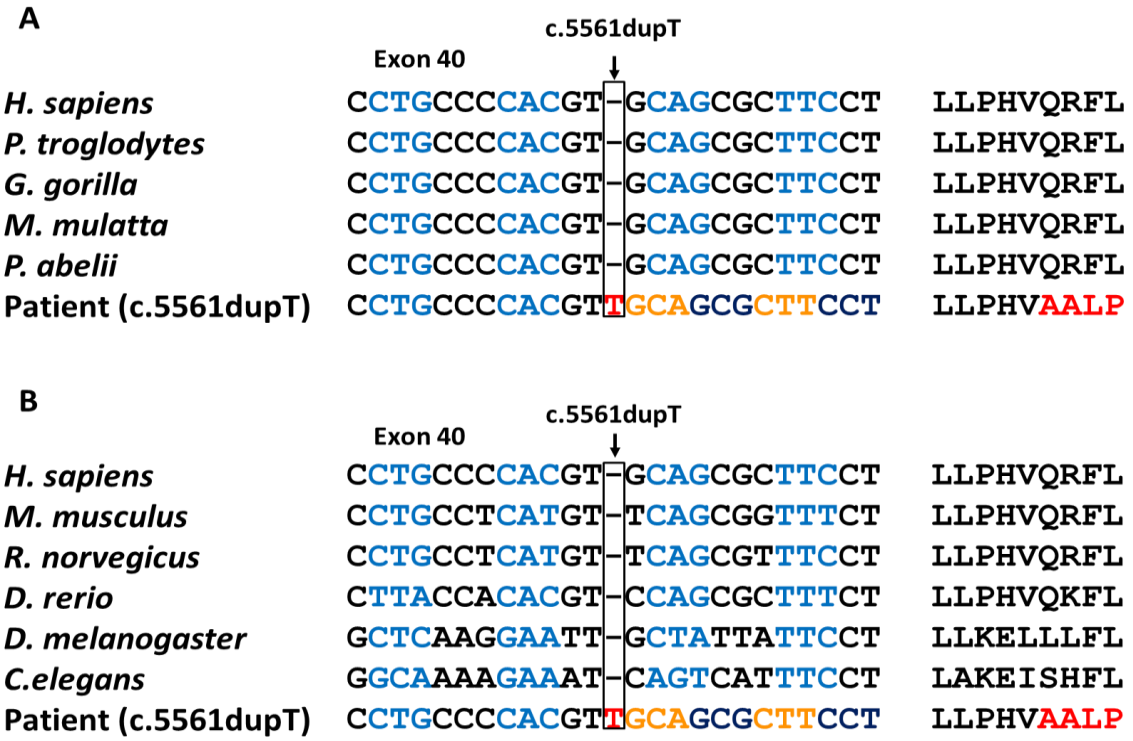

Figure 13- Nucleotide and amino acid evolutionary conservation studies for *MYO7A* gene c.5561dupT variant. A- Nucleotide and amino acid evolutionary conservation of *MYO7A* gene c.5561dupT variant in primates species. **B-** Nucleotide and amino acid evolutionary conservation of c.5561dupT variant in non-primates species.

3.2.2 Splice site prediction

Since *MYO7A* gene c.3503+1delG variant occur in the donor splice site of intron 27, it is important to study if this alteration has some influence in the normal *MYO7A* gene splicing. In Figure 14 is represented a prediction of splice site for MYO7A gene exon27 donor splice site for wt genotype and for genotype with this variant. The donor splice site prediction for wt allele show two probably positions in which splicing may occurs, while for variant allele is only presented one position which correspond to a lower scored position in the first case.

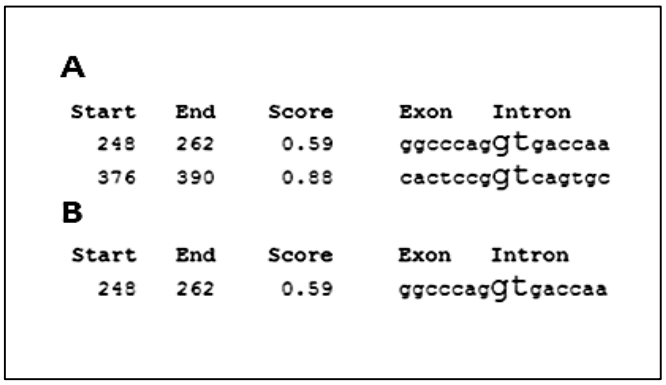

Figure 14- Splice site prediction for *MYO7A* gene exon27 donor splice site. A- Donor splice site prediction for *MYO7A* gene exon 27 wt allele. **B-** Donor splice site prediction for *MYO7A* gene exon 27 c.3503+1delG variant allele.

3.3 Transcript analyses

In order to confirm the presence of c.3503+1delG and c.5561dupT variant alleles in *MYO7A* gene transcripts, total RNA extraction from patient's and two normal individuals without USH nasal epithelium samples was performed, followed by RNA integrity number (RIN) determined with Bioanalyser (Agilent Technologies) aiming to quantify and evaluate the integrity of the extracted total RNA samples. Patient's RNA sample had a concentration of 526ng/µl, while normal individuals without USH samples showed RNA concentrations of 366ng/µl and 140ng/µl. All samples presented a RIN superior to 5 in a scale of 0 to 10 revealing a good level of integrity of total RNA samples. In detail, patient's sample had a RIN of 6.6, while normal individuals without USH samples showed a RIN of 6.8 and 6.7 (Figure 15).

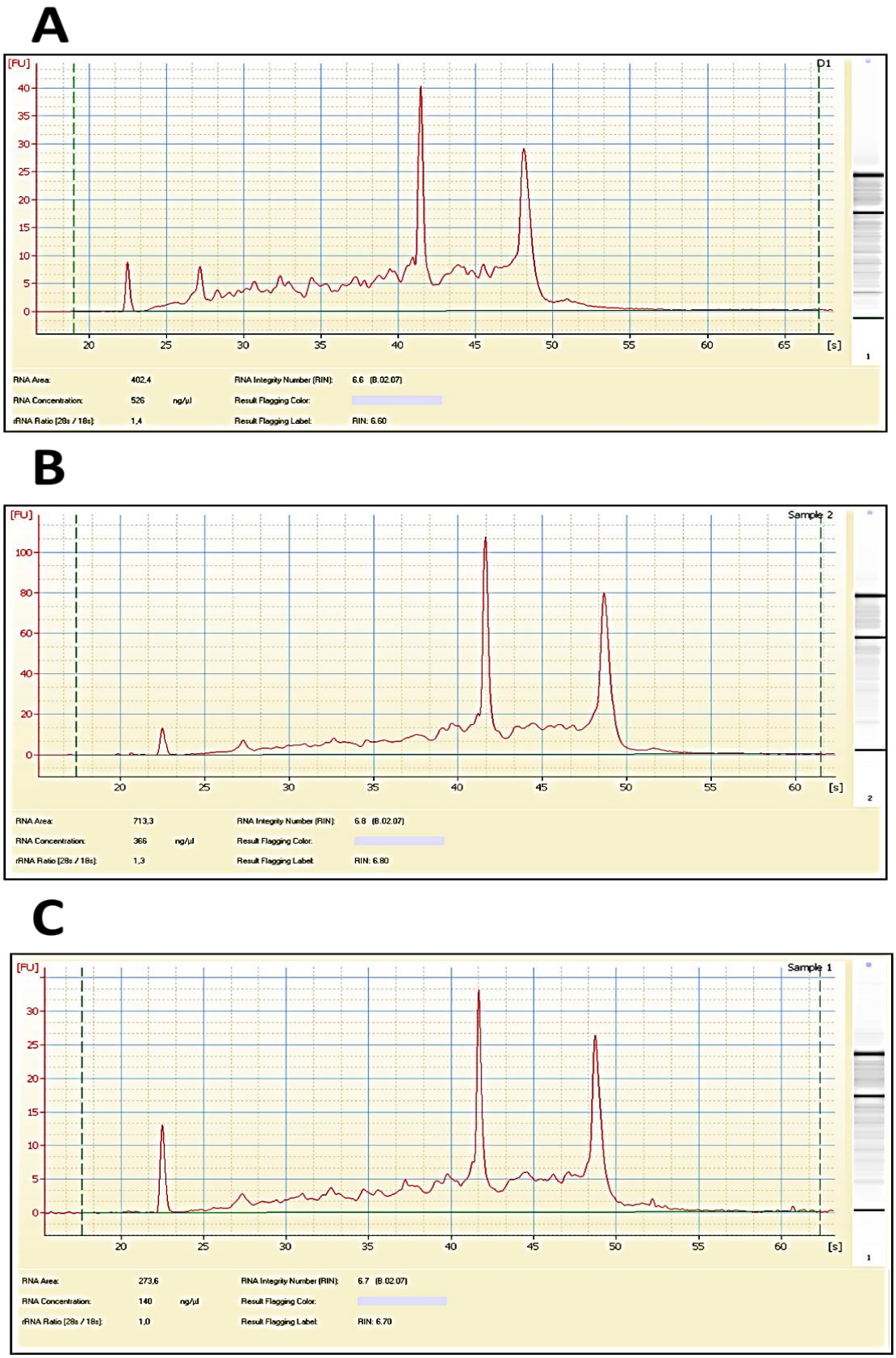

Figure 15– Total RNA quantification and integrity evaluation based on the RNA integrity number (RIN) and determined with the Bioanalyser. A- Patient´s total RNA sample (RNA concentration-526ng/µl; RIN=6.6). **B**- First normal individual without USH total RNA sample (RNA concentration-366ng/µl; RIN=6.8). **C**- Second normal individual without USH total RNA sample (RNA concentration-140ng/µl; RIN=6.7).

After RT-PCR of total RNA samples, amplification and Sequencing of *B2M* gene transcripts was performed aiming to confirm cDNA synthesis (Figure 16). Additionally, contamination with genomic DNA was discarded after failing to amplify a fragment using *MYO7A* gene intronic primers, the same as for PCR-RFLP analysis of c.5561dupT variant (Figure 17).

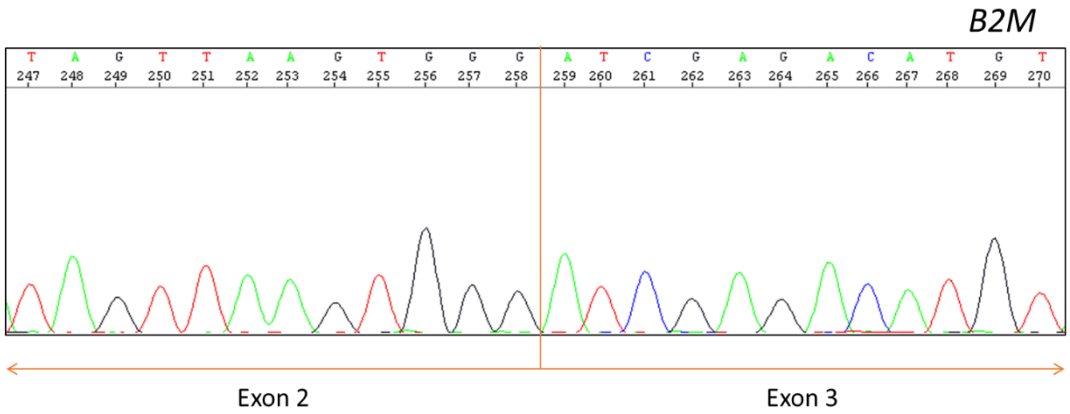

Figure 16- Electropherogram of *B2M* gene transcript. Electropherogram of the region including the end of *B2M* gene exon 2 immediately followed by the beginning of exon 3.

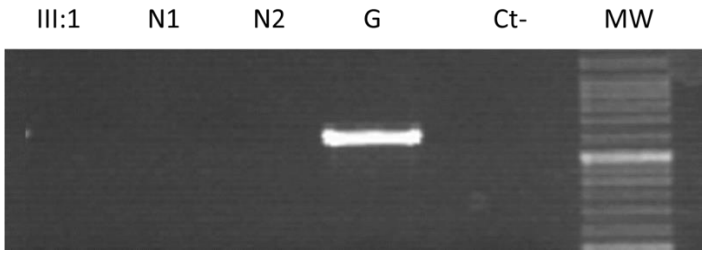

Figure 17- Photography of DNA contamination assessment in cDNA samples using *MYO7A* gene intronic primers. III:1- patient's sample; **N1 and N2-** normal individuals without USH samples. **G-** genomic DNA sample; **Ct--** PCR performed without nucleic acid sample (only with reaction mix and water) **MW-** Molecular Weight Marker NZYDNA Ladder VI (NZYTECH).

The patient and the normal individuals without USH cDNA samples were used to amplify and Sequencing *MYO7A* gene transcripts surrounding c.3503+1delG and c.5561dupT variants regions. In Figure 18 it is not possible to see any difference between the Sequencing results for c.3503+1delG variant surrounding region of patient and normal individual without USH samples. However, if it is considered the c.5561dupT variant, it is possible to read in the patient's electropherogram two overlapping sequences starting immediately after the

nucleotide c.5561, but only a single sequence in the normal individual without USH (Figure 19). This result was confirmed by PCR-RFLP, digesting the amplicon (419bp) with Eco72 I restriction enzyme and showing a lower band with 393bp for both normal individual without USH while two bands with 419bp and 393bp could be seen in the patient (Figure 20). Note that an additional fragment with 26bp was also present after digestion of the three samples but it was not visible in the electrophoresis photography.

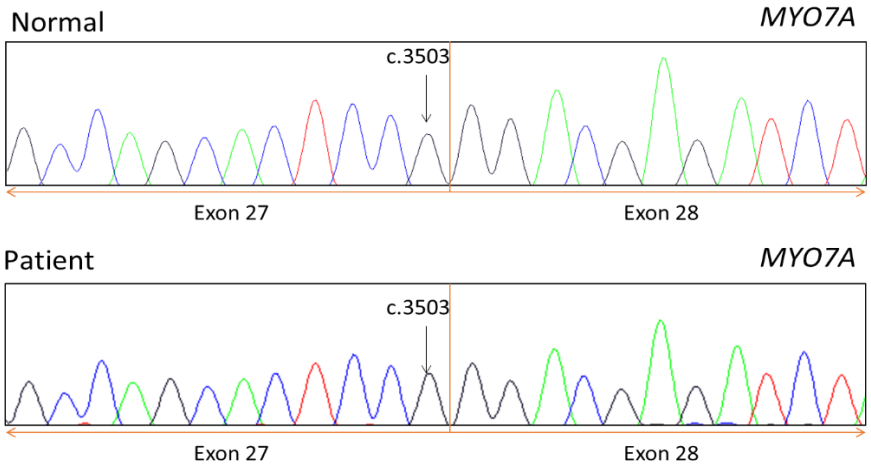

Figure 18- Electropherograms of *MYO7A* gene transcript region surrounding the c.3503 nucleotide.

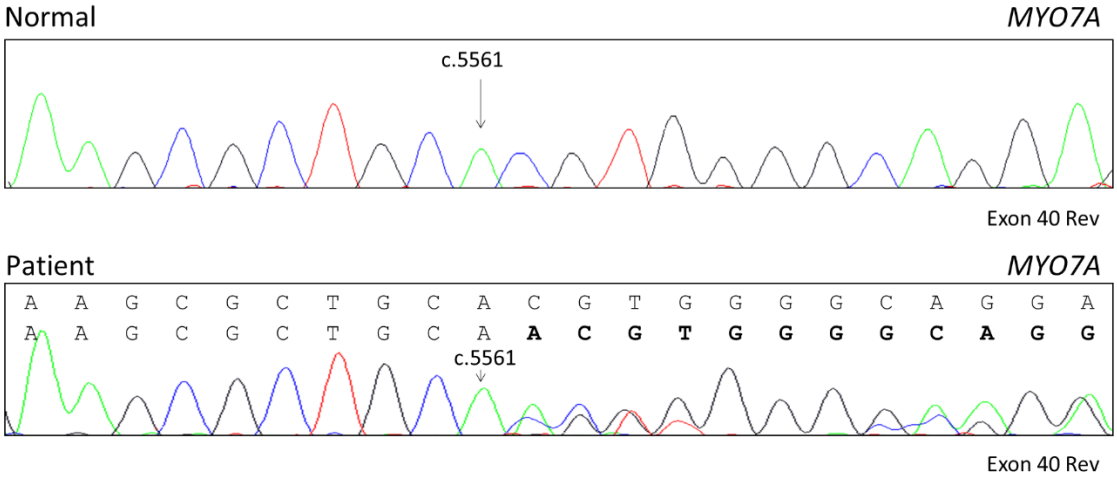

Figure 19- Electropherograms of *MYO7A* gene transcript region surrounding the c.5561 nucleotide. Note that the electropherogram is shown in the Reverse direction in order to make clear the origin of the variation.

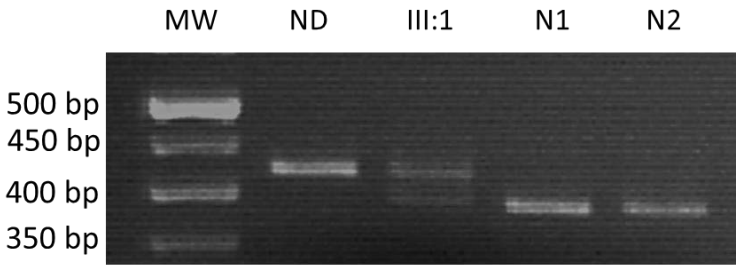

Figure 20- Photography of PCR-RFLP analysis for *MYO7A* gene nucleotide c.5561 with cDNA samples. MW- molecular weight NZYDNA Ladder VI (NZYTECH) **ND-** Non-digested sample; **III:1-** patient's sample digested with Eco72 I; **N1 and N2-** normal individuals without USH samples digested with Eco72 I.

3.4 Functional analysis

Considering that *MYO7A* gene c.5561dupT variant is located within the second MyTH4 domain of myo7a protein, and in order to understand if this variant had any influence in this protein interaction with rab-effector proteins myrip and munc13-4, some protein-protein interaction studies were performed. Accordingly, two plasmids constructions, a GFP-myo7a(F3)wt (coding for a C-terminus MyTH4-FERM wt domains with a Green fluorescent protein (GFP) tag in the N-terminus) and a GFP-myo7a(F3)mut (coding for a C-terminus MyTH4-FERM domains with a Green fluorescent protein (GFP) tag in the N-terminus but with the c.5561dupT variant inserted through Site Directed Mutagenesis techniques), were prepared and used. The proteins coded by such constructions are schematically represented in Figure 21.

The two plasmid constructions were transfected into HEK293a cells and, as anticipated, the expressed proteins had different molecular weights due to c.5561dupT variant promote the synthesis of a truncated protein (Figure 22).

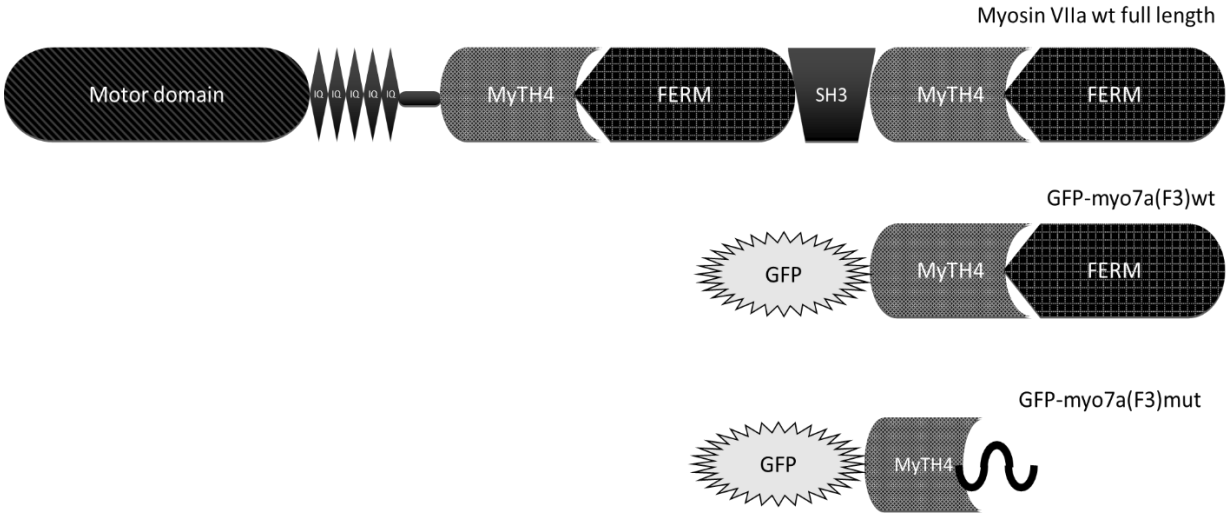

Figure 21- Schematic representation of myo7a protein constructs. In the top is represented full length myo7a protein. In the middle is represented the expected protein after GFP-myo7a(F3)wt construct expression. In the bottom is represented the expected protein after GFP-myo7a(F3)mut construct expression.

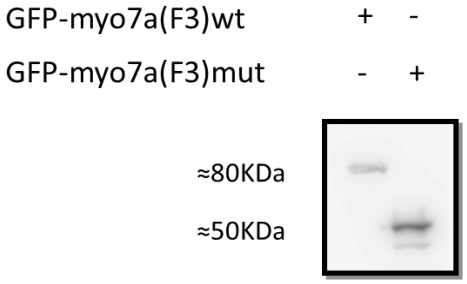

Figure 22- Expression of GFP-myo7a(F3)wt and GFP-myo7a(F3)mut. Cell lysates from HEK293A cell lines transfected with GFP-myo7a(F3)wt or GFP-myo7a(F3)mut show different molecular weights.

3.4.1 Influence of mutation in interaction between myo7a and myrip

One of the several proteins already described that interact with myo7a protein C-terminus is myrip protein. In order to verify if this interaction is disturbed by the presence of c.5561dupT variant, HEK293a cells were co-transfected with each of the previously described constructions and a plasmid construction of myrip tagged with myc, followed by IP of the cells extracts. The results revealed that in the presence of c.5561dupT variant the interaction is preserved (Figure 23). Furthermore, the distribution of myrip and both myo7a

in HEK293a cells was evaluated by immunofluorescence microscopy, revealing the co-localization of those proteins (Figure 24).

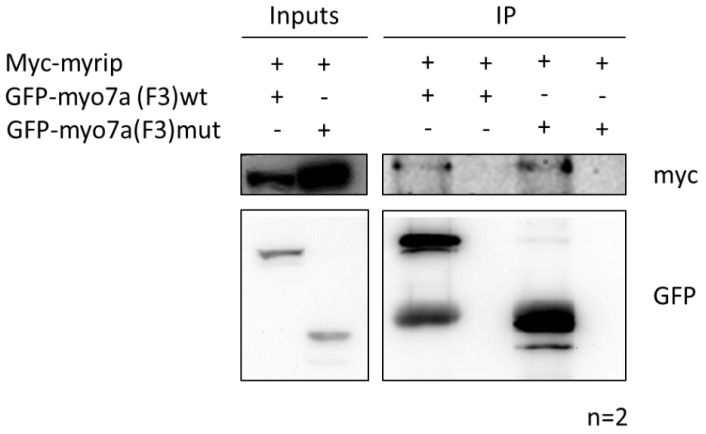

Figure 23- IP of myc-myrip and GFP-myo7a(F3)wt or GFP-myo7a(F3)mut. HEK293a cells were co-transfected with myc-myrip and GFP-myo7a(F3)wt or GFP-myo7a(F3)mut. Total levels of myc-myrip, GFP-myo7a(F3)wt and GFP-myo7a(F3)mut were evaluated by WB. GFP-myo7a(F3)wt and GFP-myo7a(F3)mut were further immunoprecipitated and the levels of myc-myrip were evaluated. Inputs represent approximately 5% of the total protein of cell lysates used for IP.

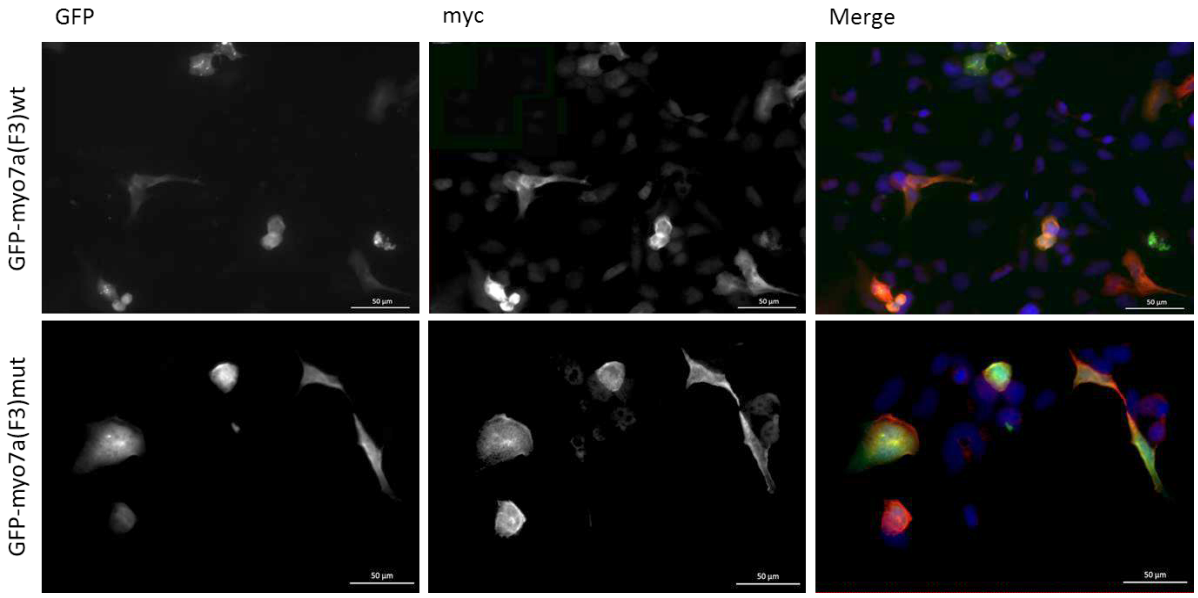

Figure 24- Immunofluorescence microscopy of myc-myrip and GFP-myo7a(F3)wt or GFP-myo7a(F3)mut. HEK293a cells were grown on fibronectin coverslips and co-transfected with myc-myrip and GFP-myo7a(F3)wt or GFP-myo7a(F3)mut. Cells were fixed with 4% PFA for 10 min and used for immunofluorescence using polyclonal antibodies directed against myc (tag). Subcellular distribution of myo7a and co-localization with myrip was further evaluated by Fluorescence microscopy. Nuclei were stained with DAPI. Scale bars, 50 μm.

3.4.2 Assessment of myo7a and munc13-4 proteins interaction in the presence or absence of c.5561dupT variant

With the purpose of assessing if proteins myo7a C-terminus and munc13-4 interact, HEK293a cells were co-transfected with munc13-4 tagged with V5 and GFP-myo7a(F3)wt or GFP-myo7a(F3)mut, followed by IP of the cells extracts. The results did not reveal any interaction between the C-terminus myo7a wt and munc13-4 proteins but, in the presence of c.5561dupT variant, it was possible to distinguish some interaction (Figure 25). Furthermore, the distribution of munc13-4 and myo7a proteins in HEK293a cells was evaluated by immunofluorescence microscopy, revealing what seems to be the co-localization of C-terminus myo7a mut and munc13-4 proteins (Figure 26).

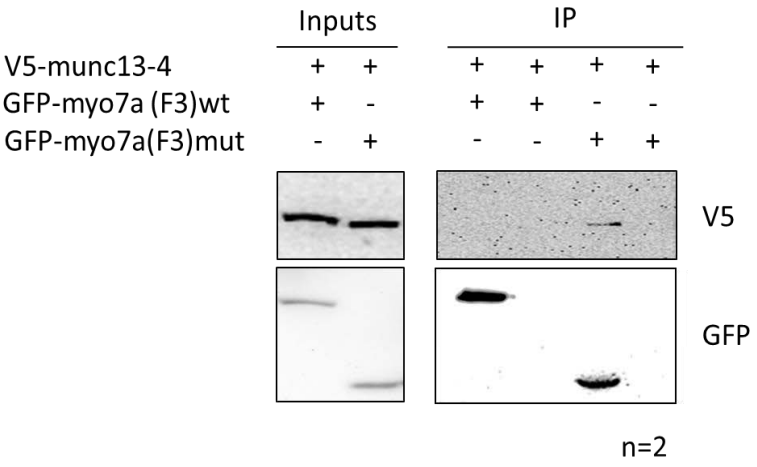

Figure 25- IP of V5-munc13-4 and GFP-myo7a(F3)wt or GFP-myo7a(F3)mut. HEK293a cells were co-transfected with V5-munc13-4 and GFP-myo7a(F3)wt or GFP-myo7a(F3)mut. Total levels of V5-munc13-4, GFP-myo7a(F3)wt and GFP-myo7a(F3)mut were evaluated by WB. GFP-myo7a(F3)wt and GFP-myo7a(F3)mut were further immunoprecipitated and the levels of V5-munc13-4 were evaluated. Inputs represent approximately 5% of the total protein of cell lysates used for IP.

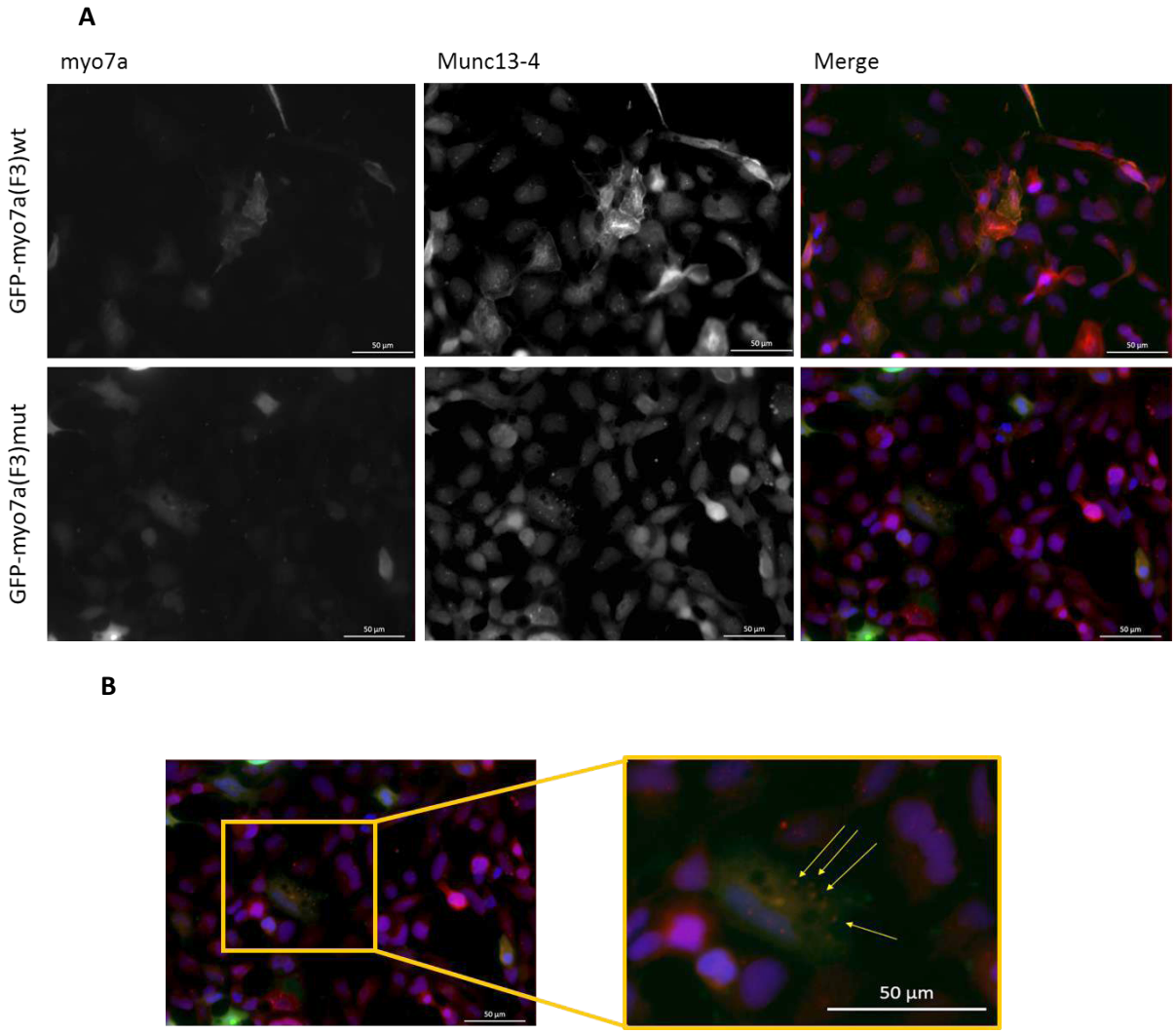

Figure 26- Immunofluorescence microscopy of V5-munc13-4 and GFP-myo7a(F3)wt or GFP-myo7a(F3)mut. A- Subcellular distribution of proteins coded by plasmids V5-munc13-4 and GFP-myo7a (F3)wt or GFP-myo7a(F3)mut. **B-** Amplification of merge image with co-localization of proteins coded by plasmids V5-munc13-4 and GFP-myo7a(F3)mut near vesicular structures (indicated with yellow arrows). HEK293a cells were grown on fibronectin coverslips and co-transfected with V5-munc13-4 and GFP-myo7a(F3)wt or GFP-myo7a(F3)mut. Cells were fixed with 4% PFA for 10 min and used for immunofluorescence using polyclonal antibodies directed against V5 (tag). Subcellular distribution of myo7a and co-localization with munc13-4 was further evaluated by Fluorescence microscopy. Nuclei were stained with DAPI. Scale bars, 50 µm.

Chapter 4

Discussion

4. Discussion

It has been estimated that 3-6 for each 100,000 persons in the world have USH (Steele-Stallard et al. 2013). The USH patients quotidian is highly restricted when compared with heathy people since two of our more important senses, vision and hearing, are impaired. In some cases, namely in USH1 patients, the congenital or during first year of life hearing loss leads to other associated limitations like speech development, further interfering in their capacity to develop social skills. The visual impairment, which normally is developed during the first decade of life, creates in these patients' additional difficulties with social skills and, in many cases, can lead to their isolation since their windows to feel and understand the world are blocked. Furthermore, the vestibular dysfunction, which is presented by some patients, affects their balance and coordination. All those aspects are responsible for patient's lower quality of life and raise a social responsibility to find solutions to the problem. In order to do so, it is necessary to understand the disease aetiology. This is the big hallmark of this study, which proposes to find the genetic mutation(s) that are responsible for USH1 in a Portuguese patient, and identify some of their functional implications at the cellular level.

After TR analysis of 9 of the known USH associated genes in an USH1 patient DNA sample and some specific *in silico* studies, two novel heterozygous possible causing disease variants in *MYO7A* gene were identified. One of these variants is c.3503+1delG exhibiting a deletion of a G at the conserved donor splice site of *MYO7A* gene intron 27 (Figure 8A). This type of variant is commonly associated to splicing events (Jaijo et al. 2011). The other variant is c.5561dupT which is a T duplication in the middle of *MYO7A* gene exon 40 (Figure 8B). This type of variant is usually associated to a frameshift error in translation that may lead to a premature stop codon (Rong et al. 2014). In this case, it is predictable that a stop codon is created 56 amino acids after the variant location, possibly originating an aberrant truncated protein in which C-terminus MyTH4 domain is incomplete and C-terminus FERM domain is totally absent. Since these two variants were found in heterozygosity and USH is defined as an autosomal recessive disease (Usher 1935), it was important to verify their segregation within the patient's family because, theoretically, they can only be responsible for the phenotype if present in the two homologous chromosomes. Additionally, five other variants (c.3503+12_33del, rs2276285, rs7927472, rs12292189 and rs2276288) identified in the patient's sample were genotyped by sequencing and PCR-RFLP studies in his relatives aiming to assist the segregation analysis of MYO7A gene c.3503+1delG and c.5561dupT variants. After these analyses it was possible to conclude that patient's chromosome 11 haplotype del-del22-C-C-A-A-N, with c.3503+1delG variant, was inherited from the mother,

and haplotype G-del22-T-T-C-T-dup, with c.5561dupT variant, was inherited from the father which in turn it is likely to have inherited from patient's paternal grandfather (Figure 10). Additionally, it was also very important to determine the frequency of the possible causing disease variants in a Portuguese population. Accordingly, the c.3503+1delG and c.5561dupT variants were not found in 250 samples from individuals without USH allowing determining a genotypic and allelic frequency of 0, supporting the hypothesis that these variants are a rare event in the Portuguese population.

In this study, the *in silico* analyses were used to give further evidences that c.3503+1delG and c.5561dupT variants are responsible or not of patient's phenotype. Therefore, evolutionary conservation studies were performed with nucleotide sequences for both variants and amino acid sequences for c.5561dupT variant using two groups of species, a group with four primate species (*P. troglodytes*, *G. gorilla*, *M. mulatta* and *P. abelii*) and a group with five non-primate species (*M. musculus*, *R. norvegicus*, *D. rerio*, *D. melanogaster* and *C. elegans*) (Figure 12 and 13). Both groups were also compared with normal *H. sapiens* and patient nucleotide and amino acid sequences surrounding variants (Figures 12 and 13). With these studies it is possible to evaluate how conserved are the analysed *loci* in species evolution, with a special emphasis in as more conserved are the *loci* among phylogenetically distant species as significant they are for the protein structure or function and as significant they are for cellular, tissue and organism homeostasis (Weil et al. 1995). Taking into consideration the c.3503+1delG variant and the surrounding nucleotide sequence, an extremely high conservation was observed among all analysed primate species and a very high conservation among the other analysed mammalian species (Figure 12), meaning that among mammals, variations in this *locus* can cause significant changes on the protein structure and function that may be associated with the USH aetiology. On the other hand, this *locus* is weakly conserved among non-mammalian species in which it is reasonably conserved in zebra fish and, virtually, not conserved in *D. melanogaster* and *C. elegans* (Figure 12). Considering the physiologic differences and the phylogenetic distance of *D. melanogaster* and *C. elegans* to human, and the association of *MYO7A* gene to USH, this result it is not very meaningful. As for c.5561dupT variant and the surrounding nucleotide and amino acid sequences, an extremely high conservation was observed in both sequences among all analysed mammalian species and in zebra fish (very high conservation in nucleotide sequence) (Figure 13) meaning that among vertebrates, variations in this *locus* can cause significant changes on the protein structure and function that may be associated with the USH aetiology. On the other hand, this *locus* is weakly conserved among *D. melanogaster* and *C. elegans* (Figure 13) in which physiologic differences and phylogenetic distance to human,

and the association of *MYO7A* gene to USH, does not give any significance for this result. Moreover, the c.3503+1deG variant is located at the donor splice site of *MYO7A* exon 27, meaning that it may be important to understand if this variant influences the RNA splicing in this *locus*. Once more computational analyses were an important tool to support the hypothesis that this variant probably is deleterious and cause USH in the studied patient. Thus, the results of splice site prediction revealed the absence of the most likely and higher score splice site for this *locus* when the variant is present (Figure 14). This type of alteration may have several implications at mRNA level, frequently associated with diseases phenotypes.

At this point, it is important to notice that both *MYO7A* gene c.3503+1delG and c.5561dupT variants are, without any doubt, mutations that, in this case, are responsible for studied patient USH phenotype as compound heterozygous mutations. This is supported by chromosome segregation in patient's family (Figure 10), mutations absence in a USH healthy population and, *in silico* evolutionary conservation data (Figures 12 and 13) and splice site prediction (Figure 14). However, the gene expression at transcript and protein levels is important for further understanding the cellular mechanisms affected by these mutations. Certainly, supplementary analyses are necessary for address such topics.

Aiming to confirm the presence of c.3503+1delG and c.5561dupT mutations in *MYO7A* gene transcripts, nasal epithelium samples were collected from the patient and two individuals without USH and total RNA samples were extracted. RNA is a thermodynamically stable molecule that can be rapidly digested in the presence of the nearly ubiquitous RNase enzymes which can compromise its applications by the fact of RNA digestion result in shorter or fewer fragments in sample (Schroeder et al. 2006), significantly affecting expression assays. To control the integrity of RNA, based on typical methods of evaluation of the ratio 28S:18S by electrophoresis, combined with microfluidics technology that provides electrophoretic separations in an automated and reproducible manner, Agilent Technologies created an algorithm that is a user-independent, automated and reliable procedure for standardization of RNA quality control allowing the calculation of an RNA integrity number (RIN) (Imbeaud et al. 2005). This algorithm classifies the RNA integrity in a range of 1 to 10, considering as acceptable samples with a RIN superior to 5 (Figure 15), a requirement fulfilled by the three extracted total RNA samples, allowing establishing the quality and quantity of such samples and proceed for the following tests.

Intending to control the efficacy of RT-PCR, a fragment of *B2M* transcript was amplified and sequenced (Figure 16) in the three cDNA samples synthetized from the extracted total RNAs with primers overlapping the end of an exon and the beginning of the

next, assuring the amplification of cDNA only. *B2M* gene codes for β2-microglobulin is a serum protein found in association with the major histocompatibility complex class I heavy chain on the surface of nearly all nucleated cells and generally found in all tissues. This is why *B2M* gene has been described as a good housekeeping gene for expression studies (Aithal and Rajeswari 2015). Another important test performed was the verification that cDNA samples were not contaminated with genomic DNA. This was done using intronic primers to amplify *MYO7A* gene exon 40 and adjacent regions, which did not show any amplification (Figure 17). Since the cDNA samples passed both tests of having cDNA and not having DNA, it was possible to proceed for *MYO7A* transcripts analysis.

The analysis of *MYO7A* transcripts in the region surrounding coding nucleotide 3503 did not reveal any difference when compared with the normal individuals without USH (Figure 18), suggesting that only the normal allele was analysed. This result could be explained by the presence of a variant in the primers binding regions. However, the primers were designed in regions known from TR analysis for not presenting any variant in patient's DNA which excluded this possibility. Another possibility is the c.3503+1delG mutation influences the transcription of an abnormal mRNA that will be degraded by a mRNA surveillance mechanism. Nevertheless, even if three of these mechanisms are already identified, only the Nonsense Mediated mRNA Decay is well known. However, it is difficult to explain the obtained result with the NMD surveillance mechanism since, after analysis of the mRNA downstream region surrounding the c.5561dupT mutation, it was possible to identify two alleles instead of one as expected after NMD. Anyway, further research is necessary to find a reasonable and reliable explanation for the suggestive result identifying only the normal sequence without any influence of the c.3503+1delG mutation after analysis of the *MYO7A* transcript surrounding region. As previously mentioned, analysis of *MYO7A* transcripts in the region surrounding the coding nucleotide 5561 revealed the presence of two overlapping sequences matching with the c.5561dupT mutation, which was not found in the normal individual without USH sample (Figure 19). Thus, the presence of c.5561dupT mutation in the *MYO7A* transcript was confirmed and it is likely that it is translated to protein influencing the normal function of the C-terminus MyTH4 domain.

Intending to evaluate if c.5561dupT mutation have any influence in the interaction between myo7a protein and the rab-effector proteins myrip and munc13-4, two GFP-myo7a plasmid constructs comprising the C-terminus MyTH4-FERM domains with and without the mutation and tagged with GFP were used (Figure 21). After both plasmid constructions transfection into HEK293a cells and respective proteins expression, it was possible to verify that the protein expressed from the GFP-myo7a(F3)mut plasmid construct showed a band

with approximately 50kDa, smaller than the protein expressed from the GFP-myo7a(F3)wt which had approximately 80kDa (Figure 22). This result supported the hypothesis that the *MYO7A* gene c.5561dupT mutation would be responsible for the presence of a premature stop codon, leading to a myo7a truncated protein.

Aiming to evaluate if, in the presence of the mutated myo7a C-terminus due to c.5561dupT mutation, the interaction with myrip protein previously reported to occur through the myo7a protein C-terminus FERM domain (discovered for the first time in 2002 in a yeast two hybrid system) (El-Amraoui et al. 2002; Ramalho et al. 2009; Schwander et al. 2009), it is still preserved. In fact and unexpectedly, it was verified that the interaction between myrip and the mutated myo7a happened (Figures 23) even with a shortened MyTH4 domain and without the FERM domain. However, the nature of this interaction was not evaluated since this experimental design does not allow confirming if this interaction occurs within the same myrip and myo7a motifs or if it is possible through different ones. Furthermore, the lower amount of myrip immunoprecipitated and the limited sensibility of WB technique does not allow to give an accurate evaluation of the ratio between the amount of myo7a protein immunoprecipitated and the amount of myrip protein immunoprecipitated, which can be different between the myo7a wt and the myo7a mut essays and, eventually, may be limiting to the purpose of this interaction (Figure 23). The study of the sub-cellular localization of both proteins was not very conclusive since the myo7a construction that was used does not have the motor domain, described as an actin binding domain responsible for the precise sub-cellular localization of the myo7a wt and myo7a mut, causing a cellular dispersed pattern for this protein. However, it is possible to verify some co-localization of both proteins when they are overexpressed in HEK293a cells which enhances the immunoprecipitation results (Figure 24).

Myo7a has been described as a motor vesicle transport protein (Lu et al. 2014). Hence, and considering that myrip and munc13-4 proteins are rab-effectors (Fukuda 2013) associated with exocytosis processes (Waselle et al. 2003; Elstak et al. 2011; Bierings et al. 2012), and that myo7a protein was associated with the lysosomes membrane at the cytoplasmic side (Soni et al. 2005), leads to the hypothesis that a possible interaction between munc13-4 and myo7a proteins may happen which, if proven, can reveal a new molecular mechanism affected in USH. The achieved results with this work refused the hypothesis since no interaction was noticeable between myo7a C-terminus wt and munc-13-4 proteins (Figure 25). But, when myo7a C-terminus presented the c.5561dupT mutation, an interaction was perceived suggesting a new acquired function for myo7a protein. Furthermore, it was verified the co-localization of C-terminus myo7a mut with munc13-4

proteins in some vesicles-like structures (Figure 26). As munc13-4 protein have been associated with lysosomes (Elstak et al. 2011) it is possible that the vesicle-like structures might be lysosomes, and it is possible to hypothesize that this possible interaction may influence the cellular lysosome-dependent events. It is also important to notice that, phagocytosis (a lysosome-dependent process) of photoreceptors outer segments by RPE has been described as a cellular process affected in *shaker1* mice, an USH animal model , and in USH patients (Gibbs et al. 2003; Gibbs et al. 2010). So far, the interaction between myo7a and munc13-4 proteins was not found in the literature raising the expectations for this work. Anyway, further research is needed to demonstrate that *MYO7A* gene c.5561dupT mutation is responsible for a myo7a protein gain of function.

Chapter 5

Final Remarks

Final remarks

In conclusion, the results of this work enable to conclude that *MYO7A gene* c.3503+1delG and c.5561dupT mutations are probably responsible for USH1 phenotype in a Portuguese patient as a compound heterozygous mutation presenting segregation among patient's family, absence in a heathy population and supported by *in silico* studies. It was not possible to detect the influence of *MYO7A gene* c.3503+1delG mutation in the nasal epithelium transcripts, but further studies are required in order to understand this result. On the opposite, *MYO7A* gene c.5561dupT mutation influence was detected in the patient's transcript. The functional studies revealed the preservation of myo7a-myrip proteins interaction in the presence of the *MYO7A gene* c.5561dupT mutation and a possible gain of function of myo7a protein C-terminus when interaction with munc13-4 protein was hypothesized. Finally, this was a truly translational multidisciplinary work since it involved the collection of patient's blood and nasal epithelium samplessamples (from bedside) and laboratory experimental research (to bench) using Molecular Genetics, Bioinformatics, Molecular Biology and Cellular Biology proceedings.

Definitely, further studies are required in order to better understand the molecular mechanisms of this disease, including realise the complex phenomenon that may be occurring at the *MYO7A* c.3503+1delG splice site. Also, an interesting subject can be the evaluation of mRNA/protein expression levels since a significant unbalance is likely to cause a deleterious phenotype. In addition, it is also required understand, not only involving the interactions between myo7a and myrip or munc13-4 proteins, but also with other proteins directly or indirectly associated with myo7a, and the possible pathogenicity of *MYO7A* gene mutations. Further studies may also include the establishment of USH transgenic animal models, in order to study the molecular and cellular features that lead to USH phenotype caused by the *MYO7A gene* mutations. Likewise, the development of genetic therapies, such as the already used in some retinal dysfunctions, may be a significant future milestone for USH research aiming to provide better and more efficient tools to improve patients quality of life.

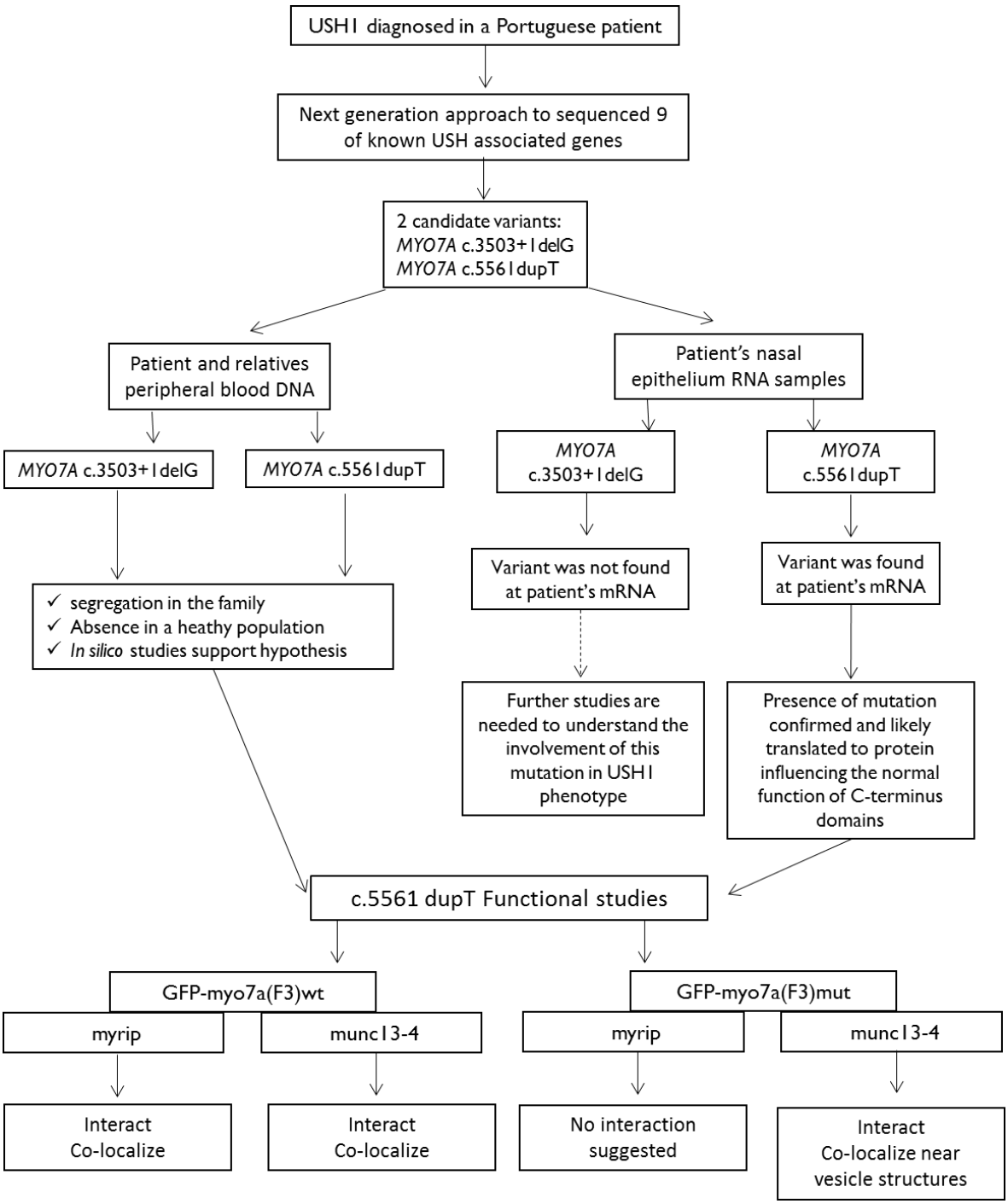

Figure 27- A Novel MYO7A Compound Heterozygous Mutation in an USH1 Portuguese Patient: a Translational Multidisciplinary Study.

Chapter 6

References

AITHAL, M. [et al.] (2015) - Validation of Housekeeping Genes for Gene Expression Analysis in Glioblastoma Using Quantitative Real-Time Polymerase Chain Reaction." Brain Tumor Res Treat" 3 (2015) 24–29.

ALAGRAMAM, K. [et al.] (2001) - Mutations in the Novel Protocadherin PCDH15 Cause Usher Syndrome Type 1F. "Human molecular genetics" 10 (2001) 1709–18.

AUSUBEL, Frederick et al. **Current Protocols in Molecular Biology.** Ringbou edition, John Wiley & Sons, Inc., 2003 ISBN: 047150338X

BAHLOUL, A. [et al.] (2009) - Vezatin, an Integral Membrane Protein of Adherens Junctions, Is Required for the Sound Resilience of Cochlear Hair Cells. "EMBO Molecular Medicine" 1 (2009) 125–38.

BIERINGS, R.[et al.] (2012) - The Interplay between the Rab27A Effectors Slp4-a and MyRIP Controls Hormone-Evoked Weibel-Palade Body Exocytosis. "Blood" 120 (2012) 2757–67.

BOËDA, B. [et al.] (2002) - Myosin VIIa, Harmonin and Cadherin 23, Three Usher I Gene Products That Cooperate to Shape the Sensory Hair Cell Bundle. "EMBO Journal" 21 (2002) 6689–99.

BOLZ, H [et al.] (2001) - Mutation of CDH23, Encoding a New Member of the Cadherin Gene Family, Causes Usher Syndrome Type 1D. "Nature genetics" 27 (2001) 108–12.

BOSCO, A. [et al.] (2011) - Early Microglia Activation in a Mouse Model of Chronic Glaucoma. "Journal of Comparative Neurology" 519 (2011) 599–620.

CIUMAN, R. (2013) - Inner Ear Symptoms and Disease: Pathophysiological Understanding and Therapeutic Options. "Medical science monitor : international medical journal of experimental and clinical research" 19 (2013) 1195–1210.

DAI, H. [et al.] (2008) - Identification of Five Novel Mutations in the Long Isoform of the USH2A Gene in Chinese Families with Usher Syndrome Type II. "Molecular vision" 14 (2008) 2067–75.

DAIGER, S [et al.] (2013) - Genes and Mutations Causing Retinitis Pigmentosa. "Clinical Genetics" 84 (2013) 132–41.

DALLOS, P [et al.] (1992) - The Active Cochlea. "The Journal of neuroscience : the official journal of the Society for Neuroscience" 12 (1992) 4575–85.

EATOCK, R. [et al.] (2011) - Vestibular hair cells and afferents: two channels for head motion signals. "Annual review of neuroscience" 34 (2011) 501-534

EBERMANN, I. [et al.] (2007) - A Novel Gene for Usher Syndrome Type 2: Mutations in the Long Isoform of Whirlin Are Associated with Retinitis Pigmentosa and Sensorineural Hearing Loss. "Human Genetics" 121 (2007) 203–11.

EBNETER, A. [et al.] (2015) - Metrics of the Normal Anterior Sclera: Imaging with Optical Coherence Tomography. "Graefe's Archive for Clinical and Experimental Ophthalmology" (2015).

EL-AMRAOUI, A. [et al.] (2002) - MyRIP, a Novel Rab Effector, Enables Myosin VIIa Recruitment to Retinal Melanosomes. "EMBO Reports" 3 (2002) 463–70.

EL-AMRAOUI, A. [et al.] (2005) - Usher I Syndrome: Unravelling the Mechanisms That Underlie the Cohesion of the Growing Hair Bundle in Inner Ear Sensory Cells. "Journal of cell science" 118 (2005) 4593–4603.

ELSTAK, E. [et al.] (2011) - The munc13-4-rab27 Complex Is Specifically Required for Tethering Secretory Lysosomes at the Plasma Membrane. "Blood" 118 (2011) 1570–78.

ERSKINE, L. [et al.]. 2014. Connecting the Retina to the Brain. "ASN Neuro" 6 (2014) 1–26.

ETOURNAY, R. [et al.] (2005) - PHR1, an Integral Membrane Protein of the Inner Ear Sensory Cells, Directly Interacts with Myosin 1c and Myosin VIIa. "Journal of cell science" 118 (2005) 2891–99.

ETOURNAY, R. [et al.] (2007) - Shroom2, a Myosin-VIIa- and Actin-Binding Protein, Directly Interacts with ZO-1 at Tight Junctions. "Journal of cell science" 120 (2007) 2838–50.

EUDY, J. [et al.] (1998) - Mutation of a Gene Encoding a Protein with Extracellular Matrix Motifs in Usher Syndrome Type IIa. "Science" 280 (1998) 1753–57.

FRIEDMAN, T. [et al.] (2011) - Usher Syndrome: Hearing Loss with Vision Loss. " Medical Genetics in the Clinical Practice of ORL" 70 (2011) 56–65.

FUKUDA, M. [et al.] (2013) - Rab27 Effectors, Pleiotropic Regulators in Secretory Pathways. "Traffic" 14 (2013) 949–63.

GELI, M. [et al.] (2000) - An Intact SH3 Domain Is Required for Myosin I-Induced Actin Polymerization. "The EMBO journal" 19 (2000) 4281–91.

GIBBS, D. [et al.] (2010) - Function of MYO7A in the Human RPE and the Validity of Shaker1 Mice as a Model for Usher Syndrome 1B and Immunolabeling of Retinal Sections. "Retinal Cell Biology" 51 (2010) 1130–35.

GIBBS, D. [et al.] (2003) -. Abnormal Phagocytosis by Retinal Pigmented Epithelium That Lacks Myosin VIIa, the Usher Syndrome 1B Protein. "Proceedings of the National Academy of Sciences of the United States of America" 100 (2003) 6481–86.

GILLESPIE, P. [et al.] (2002) - Myosin-VIIa and Transduction Channel Tension. "Nature neuroscience" 5 (2002) 3–4.

GRAEFE, A. (1858) - Vereinzelte Beobachtugen und Bemerkugen exceptionelle verhalten des Gesichsfeldes bei Pigmentartung des Netzhaut. "Archives in Klinicheskaia Ophthalmology" 4 (1858) 250-3.

HOLT, J. [et al.] (2007) - Assessment of Myosin II, Va, VI and VIIa Loss of Function on Endocytosis and Endocytic Vesicle Motility in Bone Marrow-Derived Dendritic Cells. "Cell Motility and the Cytoskeleton" 64 (2007) 756–66.

IMBEAUD, S. [et al.] (2005) - Towards Standardization of RNA Quality Assessment Using User-Independent Classifiers of Microcapillary Electrophoresis Traces. "Nucleic Acids Research" 33 (2005) 1–12.

JAIJO, T [et al.] (2011) - Functional Analysis of Splicing Mutations in MYO7A and USH2A Genes. "Clinical Genetics" 79 (2011) 282–88.

JOENSUU, T. [et al.] (2001) - Mutations in a Novel Gene with Transmembrane Domains Underlie Usher Syndrome Type 3. "American journal of human genetics" 69 (2001) 673–84.

KEATS, B. [et al.] (2000) - The Usher Syndromes. "American Journal of Human Genetics" 166 (2000) 158–66.

KEATS, B. [et al.] (2004) - Genetic Heterogeneity in Usher Syndrome. "American journal of medical genetics. Part A" 130A (2004) 13–16.

KHAN, S. and CHANG, R. (2013) - Anatomy of the Vestibular System: A Review. "NeuroRehabilitation" 32 (2013) 437–43.

KOLB, H. (1991). Simple Anatomy of the Retina. " Webvision The Organization of the Retina and Visual System" (1991).

KOLB, H. (2005) - Gross Anatomy of the Eye. "Webvision The Organization of the Retina and Visual System" (2005).

KÜSSEL-ANDERMANN, P. [et al.] (2000) - Unconventional Myosin VIIA Is a Novel A-Kinase-Anchoring Protein. "Journal of Biological Chemistry" 275 (2000) 29654–59.

LEMASURIER, M. and GILLESPIE, P. (2005) - Hair-Cell Mechanotransduction and Cochlear Amplification. "Neuron" 48 (2005) 403–15.

LEVIS, H. [et al.] (2015) - Tissue Engineering the Cornea: The Evolution of RAFT. "Journal of Functional Biomaterials" 6 (2015) 50–65.

LIU, F. [et al.] (2013) - Novel Compound Heterozygous Mutations in MYO7A in a Chinese Family with Usher Syndrome Type 1. "Molecular vision" 19 (2013) 695–701.

LIU, X. [et al.] (1999) - Myosin VIIa Participates in Opsin Transport through the Photoreceptor Cilium. "The Journal of neuroscience : the official journal of the Society for Neuroscience" 19 (1999) 6267–74.

LIU, X. [et al.] (2015) - Progress in Histopathologic and Pathogenesis Research in a Retinitis Pigmentosa M. "Histology and Histopathology" 30 (2015) 771–79.

LU, Q. [et al.] (2014) - Cargo Recognition and Cargo-Mediated Regulation of Unconventional Myosins. "Accounts of chemical research" 47 (2014) 3061-70.

LULL, M. and BLOCK, M. (2010) - Microglial Activation and Chronic Neurodegeneration. "Neurotherapeutics" 7 (2010) 354–65.

MASON, J. and HERRMANN, K. (1998) - Response Measurement. "Pediatrics" 101 (1998) 221-228.

MATHUR, P. and YANG, J. (2015) - Usher Syndrome: Hearing Loss, Retinal Degeneration and Associated Abnormalities. "Biochimica et Biophysica Acta (BBA) - Molecular Basis of Disease" 1852 (2015) 406–20.

MILLÁN, J. [et al.] (2011) - An Update on the Genetics of Usher Syndrome. "Journal of ophthalmology" 2011 (2011) 417217.

NICKLA, D. and WALLMAN, J. (2010) - The Multifunctional Choroid. "Progress in Retinal and Eye Research" 29 (2010) 144–68.

PERLMAN, I. [et al.] (2012) - S-Potentials and Horizontal Cells "Webvision The Organization of the Retina and Visual System" (2012): 1–110.

PETIT, C. (2001) - Usher Syndrome: From Genetics to Pathogenesis. "Annual review of Human Genomics Human Genetics" (2001) 271-97.

PETRASH, J. (2013) - Aging and Age-Related Diseases of the Ocular Lens and Vitreous Body. "Investigative Ophthalmology and Visual Science" 54 (2013) 54–59.

PFEIFFER, C. [et al.] (2014) The Vestibular System: A Spatial Reference for Bodily Self-Consciousness. "Frontiers in integrative neuroscience" 8 (2014) 31.

PHATNANI, H., and MANIATIS, T. (2015) - Astrocytes in Neurodegenerative Disease. "CSH Prespectives in Biology" (2015) 1–18.

PURVES, DALE ET AL. - **NEUROSCIENCE**. THIRD EDITION. SUNDERLAND, MASSACHUSETTS,USA. SINAUER ASSOCIATES, INC, 2004 ISBN 0-87893-725-0

RAMALHO, J. [et al.] (2009) - Myrip Uses Distinct Domains in the Cellular Activation of Myosin VA and Myosin VIIA in Melanosome Transport. "Pigment Cell and Melanoma Research" 22 (2009) 461–73.

REICHENBACH, A. and BRINGMANN, A. (2013) - New Functions of Müller Cells. "Glia" 61 (2013) 651–78.

RIAZUDDIN, S. [et al.] (2012) - Alterations of the CIB2 Calcium- and Integrin-Binding Protein Cause Usher Syndrome Type 1J and Nonsyndromic Deafness DFNB48. "Nature Genetics" 44 (2012) 1265–71.

RONG, W. [et al.] (2014) - Novel and Recurrent MYO7A Mutations in Usher Syndrome Type 1 and Type 2. "PLoS ONE" 9 (2014).

ROSA, J. [et al.] (2015) - Neuron-Glia Signaling in Developing Retina Mediated by Neurotransmitter Spillover. "eLIFE" (2015).

SAKAI, T. [et al.] (2011) - Cargo Binding Activates Myosin VIIA Motor Function in Cells. "Proceedings of the National Academy of Sciences of the United States of America" 108 (2011) 7028–33.

SCHRIJVER, I. and GARDNER, P. (2006) - Hereditary Sensorineural Hearing Loss: Advances in Molecular Genetics and Mutation Analysis. "Expert review of molecular diagnostics" 6 (2006) 375–86.

SCHROEDER, A. [et al.] (2006) - The RIN: An RNA Integrity Number for Assigning Integrity Values to RNA Measurements. "BMC molecular biology" 7 (2006).

SCHWANDER, M. [et al.] (2009) - A Novel Allele of Myosin VIIa Reveals a Critical Function for the C-Terminal FERM Domain for Melanosome Transport in Retinal Pigment Epithelial Cells. "The Journal of neuroscience : the official journal of the Society for Neuroscience" 29 (2009) 15810–18.

SLEPECKY, N. (1996) - Structure of the Mammalian Retina. "Springer Handbook of Auditory Research" 8 (1996) 44–129.

SONI, L. [et al.] (2005) - The Unconventional Myosin-VIIa Associates with Lysosomes. "Cell Motility and the Cytoskeleton" 62 (2005) 13–26.

STEELE-STALLARD, H. [et al.] (2013) - Screening for Duplications, Deletions and a Common Intronic Mutation Detects 35% of Second Mutations in Patients with USH2A Monoallelic Mutations on Sanger Sequencing. "Orphanet journal of rare diseases" 8 (2013) 122.

SWEENEY, L. and HOUDUSSE, A. (2010) - Structural and Functional Insights into the Myosin Motor Mechanism. "Annual review of biophysics" 39 (2010) 539–57.

USHER, C. (1935) - Bowman's Lecture: On a Few Hereditary Eye Affections. "Transactions of the Ophthalmological Societies of the United Kingdo" 55 (1935) 164–245.

VACHÉ, C. [et al.] (2010) - Nasal Epithelial Cells Are a Reliable Source to Study Splicing Variants in Usher Syndrome. "Human Mutation" 31 (2010) 734–41.

VASTINSALO, H. [et al.] (2006) - Two Finnish USH1B Patients with Three Novel Mutations in Myosin VIIA. "Molecular vision" 12 (2006) 1093–97.

VERPY, E. [et al.] (2000) - A Defect in Harmonin, a PDZ Domain-Containing Protein Expressed in the Inner Ear Sensory Hair Cells, Underlies Usher Syndrome Type 1C. "Nature genetics" 26 (2000) 51–55.

WANG, J. (2015) - Functions of Müller Cell-Derived Vascular Endothelial Growth Factor in Diabetic Retinopathy. "World Journal of Diabetes" 6 (2015) 726-33.

WANG, Q. [et al.] (2007) - The SH3 Domain of a M7 Interacts with Its C-Terminal Proline-Rich Region. "Protein science : a publication of the Protein Society" 16 (2007) 189–96.

WASELLE, L. [et al]. (2004) - Involvement of rab27 Binding Protein Slac2c/myrip in insulin exocytosis. "Molecular biology of the cell" 14 (2003) 4103-4113.

WEIL, D. [et al.] (1995) - Defective Myosin VIIA Gene Responsible for Usher Syndrome Type 1B. "Nature" 374(1995): 60–61.

WEIL, D. [et al.] (2003) - Usher Syndrome Type I G (USH1G) Is Caused by Mutations in the Gene Encoding SANS, a Protein That Associates with the USH1C Protein, Harmonin. "Human Molecular Genetics" 12 (2003) 463–71.

WESTON, M. [et al.] (2004) - Mutations in the VLGR1 Gene Implicate G-Protein Signaling in the Pathogenesis of Usher Syndrome Type II. "American journal of human genetics" 74 (2004) 357–66.

WILLIAMS, D. (2002) - Transport to the Photoreceptor Outer Segment by Myosin VIIa and Kinesin II. "Vision Research" 42 (2002) 455–62.

WILLIAMS, D. and LOPES, V. (2011) - The Many Different Cellular Functions of MYO7A in the Retina. "Cellular Cytoskeletal Motor Proteins" 39 (2011) 1207–10.

WOLFRUM, U. and SCHMITT, A. (2000) - Rhodopsin Transport in the Membrane of the Connecting Cilium of Mammalian Photoreceptor Cells. "Cell Motility and the Cytoskeleton" 46 (2000) 95–107.

WONG, A. and RYAN, A. (2015) - Mechanisms of Sensorineural Cell Damage, Death and Survival in the Cochlea. "Frontiers in Aging Neuroscience" 7 (2015) 1–15.

YODER, R. and TAUBE, J. (2014) - The Vestibular Contribution to the Head Direction Signal and Navigation. "Frontiers in integrative neuroscience" 8 (2014) 32.

YOUNG, RICHARD W. 1967. The Renewal of Photoreceptors Cell Outer Segments. (1967): 61–72.

YOUNG, R. and BOK, D. (1969). Participation of the Retinal Pigment Epithelium in the Rod Outer Segment Renewal Process. "Journal of Cell Biology" 42 (1969) 392–403.